Eur. Phys. J. Plus (2025) 140:551
https://doi.org/10.1140/epjp/s13360-025-06481-z

THE EUROPEAN PHYSICAL JOURNAL PLUS

Regular Article

Network-based SEITR epidemiological model with contact heterogeneity: comparison with homogeneous models for random, scale-free and small-world networks

Selim Karaoglu[a], **Muhammad Imran**[b], **Brett A. McKinney**[c]

Tandy School of Computer Science, The University of Tulsa, 800 South Tucker Drive, Tulsa, OK, USA

Received: 14 March 2025 / Accepted: 26 May 2025

Abstract The spread of infectious diseases can be accurately modeled using differential equations, but these models assume the contacts between individuals are homogeneous. Network methods, on the other hand, can account for variation of contacts between individuals. We introduce a new network-based epidemiological modeling algorithm for a susceptible-exposed-infected-treated-recovered (SEITR) model. The epidemiological parameters of the network model map to the homogeneous ODE model parameter for comparison. We use a range of simulated rate constants and random network distributions to directly compare the heterogeneous network-based approach and the homogeneous ODE model. We simulate SEITR models on Erdős–Renyi, Barabási–Albert, and Watts–Strogatz networks with various sizes and connectivities. Among these networks, Watts–Strogatz networks exhibit the largest deviations from the homogeneous model, highlighting the importance of this network structure in influencing disease dynamics. We use the same parametric values in the network-based algorithm as in the compartmental ODE model, and find notable differences for the infectious compartment due to network effects. We demonstrate the utility of this approach on a realistic model of lumpy skin disease (LSD) transmission dynamics, which can be extended to other infectious diseases. The heterogeneous network-based SEITR model provides novel insights into LSD transmission, and the network method provides a valuable tool for researchers to model deviation from the homogeneous assumptions for other viruses.

1 Introduction

Compartmental modeling is an important tool to understand epidemic dynamics and formulate optimal control strategies [1–3]. These mathematical models find widespread application in the study of various diseases such as COVID-19, tuberculosis [1], dengue [2], malaria [3], HBV disease [4], foot and mouth disease [5], and lumpy skin disease (LSD) [6, 7]. Numerous extended *SIR* mathematical models have been proposed in the literature for different epidemic diseases [6–9]. In the work by [6], the authors introduce a vaccination compartment and define an optimal control problem for LSD dynamics. The implementation of cattle treatment, along with its limitations, was analyzed in a separate study [7]. Another study extending the *SIR* model by incorporating a vaccination compartment and rate, explored the interaction of infectious vectors and cattle as control strategies [9]. The above-mentioned models, utilize a nonlinear system of differential equations with homogeneous mixing assumptions for the dynamics of the epidemic [6–8]. Our contribution extends network-based epidemic modeling to susceptible-exposed-infected-treated-recovered (*SEITR*), offering a perspective that accounts for complex interactions beyond the homogeneous compartment model approach.

The foundations of epidemiology and early epidemiological models were based on population-wide random mixing [10–13]. However, in practical terms, each individual possesses a finite set of contacts through which they can transmit infection [14, 15]. The collective set of all such contacts constitutes a mixing network [15, 16]. The crucial concern revolves around the presence of individual relationships in a population [16]. The onset of an outbreak occurs when one or more nodes become infected from outside the population, termed imported infections. The ultimate size of an outbreak is determined by the number of nodes infected before transmission is complete. Many *SIR* mathematical models have been developed with the assistance of networks following the COVID-19 pandemic [10, 13, 15, 17]. These models utilize random and scale-free networks to analyze the effects of connections, specifically focusing on the degree distribution of nodes [14, 18]. Many network-based mathematical models for different diseases are available in the literature [15–17, 19]. Network approaches focus on heterogeneity by considering contact variations among

[a] e-mail: selim-karaoglu@utulsa.edu
[b] e-mail: muhammad-imran@utulsa.edu (corresponding author)
[c] e-mail: brett-mckinney@utulsa.edu

Published online: 18 June 2025

individuals or groups within a population in the modeling of the spread of infectious diseases and the demographic property (i.e., the presence of birth and death rates).

Our objective is to model the dynamics of LSD outbreak using a *SEITR* (susceptible-exposed-infected-treatment-recovered) model with various random networks. The representation of the cattle population takes the form of a graph, where each node signifies an individual and edges symbolize encounters between them. The state of each individual (node) is categorized as susceptible (S), exposed (E), infected (I), under-treatment (T), and recovered (R), with the total population (N) being the sum of individuals in all states. The simulation is executed multiple times, each run depicting a different realization of the disease outbreak. In each run, disease dynamics unfold over a specified number of time steps. At the initiation of each run, the population graph is primed with a specified number of individuals in each state; this number can be adjusted for different experiments.

Real social networks do not have a clear structure but may have certain patterns. Therefore, to describe them approximately it is common practice to use random graph models of complex networks [19]. We experimented with three different types of network graphs: Erdős–Rényi, Barabási–Albert, and Watts–Strogatz. Each of these networks represents unique topological characteristics that are often observed in real-world scenarios, making them ideal for this analysis [18, 19]. The Erdős–Rényi network is a type of random graph where each edge has an equal probability of being present or absent, independent of the other edges [20]. This randomness can mirror certain real-world networks where connections are formed independently. The Barabási–Albert network, on the other hand, is a scale-free network that follows the principle of preferential attachment. This principle, which is frequently observed in real-world networks, states that the more connected a node is, the more likely it is to receive new links. Networks such as the internet, social networks, and protein interactions often exhibit such scale-free properties [21]. Lastly, the Watts–Strogatz network models the small-world property, a key characteristic of many real-world networks. Small-world networks are characterized by a high clustering coefficient and small path length, representing networks where nodes are not all directly linked but most can be reached from each other by a small number of hops or steps [22]. These network structures introduce varying degrees and types of contact heterogeneity. Erdős–Rényi networks typically display relatively uniform contact patterns, while Barabási–Albert networks exhibit significant degree heterogeneity: few nodes (hubs) have a large number of connections, while the majority have very few. Watts–Strogatz networks combine local clustering with short average path lengths, introducing structured randomness that can still support clustered transmission pathways. This heterogeneity influences the spread of the disease throughout the network. In our simulations, we observed that Watts–Strogatz networks, due to their clustered and rewired edges, deviated most significantly from the homogeneous compartmental model in terms of infection dynamics. Such deviations underscore the importance of incorporating topological features when modeling infectious diseases. The selection of these networks is crucial, as it allows for a comprehensive evaluation of the *SEITR* model across diverse network structures. It enables us to understand how the model performs under different conditions and how changes in network structure can impact disease dynamics.

We provide an SEITRNet R library that includes functions for simulation and analysis on GitHub.[1] To apply the *SEITR* model, we create various networks by alternating network types, sizes, and parameters. In addition to these networks, the implementation considers newborn members, naturally deceased members, and members deceased due to infection. We assign status transitions for born and deceased nodes based on the parameters of our *SEITR* model. The manuscript is organized as follows: Sect. 2.1 consists of the formulation of the homogeneous network models for LSD and associated properties. In Sect. 2.2, we describe the network SEITR algorithm and compare different experiments on random networks with corresponding homogeneous models. The SEITR model simulation results are presented in Sect. 3, and the conclusion and future direction are given in Sect. 4.

2 Methods

2.1 Well-posed SEITR mathematical model

Here we describe the homogeneous *SEITR* model designed for the analysis of lumpy skin disease (LSD). The total population $N(t)$ is categorized into five distinct groups: susceptible $S(t)$, exposed $E(t)$, infected $I(t)$, under-treatment $T(t)$, and recovered or removed $R(t)$. The susceptible group $S(t)$ comprises cattle vulnerable to the virus, capable of falling ill after exposure to an infectious interaction. The exposed group $E(t)$ consists of individuals who have contracted the virus but remain asymptomatic and non-contagious. As the virus establishes itself in an exposed cow, the cow transitions into the infected group $I(t)$. Cattle infected with the disease can transmit it to otherwise healthy herds. The under-treatment class $T(t)$ encompasses cattle undergoing medical interventions for LSD, constituting individuals subjected to prompt recovery therapies. The recovered class $R(t)$ includes cattle successfully treated or those who have developed natural immunity to the infectious disease. The detailed formulation of this model can be found in [7], which outlines the system of non-linear differential equations governing these dynamics. The transmission and translation of the LSD model (Eq. 1) can be seen in Fig. 1.

$$\frac{dS}{dt} = \Lambda - \frac{\beta_1 SI}{N} - \mu S, \tag{1a}$$

[1] The R library SEITRNet can be accessed at: https://github.com/insilico/SEITRNet.

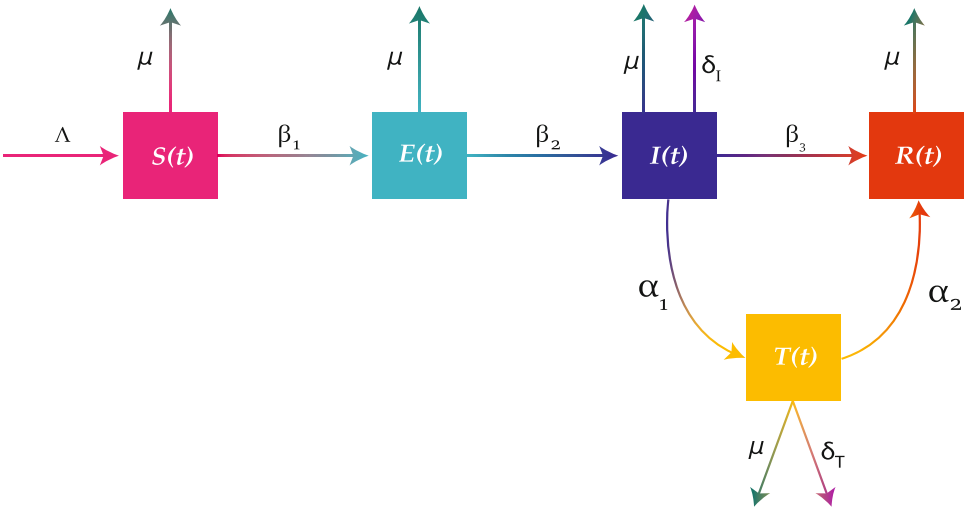

Fig. 1 Flow diagram of LSD transmission and translation within the compartments

$$\frac{dE}{dt} = \frac{\beta_1 SI}{N} - (\beta_2 + \mu)E, \tag{1b}$$

$$\frac{dI}{dt} = \beta_2 E - (\beta_3 + \alpha_1 + \delta_I + \mu)I, \tag{1c}$$

$$\frac{dT}{dt} = \alpha_1 I - (\mu + \delta_T + \alpha_2)T, \tag{1d}$$

$$\frac{dR}{dt} = \beta_3 I + \alpha_2 T - \mu R, \tag{1e}$$

with non-negative initial conditions

$$S(0) = S_0 > 0,\ E(0) = E_0 \geq 0,\ I(0) = I_0 \geq 0,\ T(0) = T_0 \geq 0,\ R(0) = R_0 \geq 0. \tag{1f}$$

Details of the following theorems can be found in Ref. [7].

Theorem 1 *The LSD model (Eq. 1) has a unique solution.*

Theorem 2 *The solution* $y(t) = (S(t), E(t), I(t), T(t), R(t))$ *of the LSD model (Eq. 1) is positive for all time* $t \geq 0$ *given nonnegative initial conditions.*

Theorem 3 *The solution* $y(t) = (S(t), E(t), I(t), T(t), R(t))$ *of the LSD model (Eq. 1) is bounded by* $\frac{\Pi}{\mu}$.

Theorem 4 *The LSD model (Eq. 1) is LAS (locally asymptotically stable) and GAS (globally asymptotically stable) at the disease-free equilibrium point.*

Theorem 5 *The endemic equilibrium point of model (Eq. 1) is locally and globally asymptotically stable.*

The SEITR model uses the following parameters.

- Λ : Birth or recruitment rate.
- β_1 : Interaction between susceptible and infected cattle.
- β_2 : Translation rate from exposed to infected.
- β_3 : Recovery rate of the infected cattle.
- α_1 : Treatment rate of infected cattle.
- α_2 : Recovery rate of under-treatment cattle.
- δ_I : Death due to LSD in infected cattle.
- δ_T : Death due to LSD in under-treatment cattle.
- μ : Natural death rate.

2.2 SEITR network simulation algorithm

Algorithm 1 Multiple (num_exp) experiments of the network simulation

Require: Network Type, n, n_par1[1], n_par2[2], Λ, β_1, β_2, β_3, α_1, α_2, δ_I, δ_T, μ, S, E, I, T, R, N, t, *num_exp*

for each experiment in num_exp experiments **do**
  Create network g with given parameters, e.g., ER, WS or BA
  Assign statuses to nodes randomly
  for each time step t in the simulation **do**
    Save the current status in *S_count*, *E_count*, *I_count*, *T_count*, *R_count*, *N_count*
    for each type of removal (Infection: $\delta_I * I\_count$, Treatment: $\delta_T * T\_count$, natural death: $\mu * N$) **do**
      Set *nodes_to_remove_count* for removal type
      Separate *nodes_to_remove_count* into a $floor\_value$ and a $fractional\_part$
      if $floor\_value > 0$ **then**
        Remove random $floor\_value$ number of nodes
      end if
      if $fractional\_part > 0$ & $rand \in [0,1) < fractional\_part$ **then**
        Remove an additional random node
      end if
    end for
    $nodes\_to\_add\_count = \Lambda$
    Separate *nodes_to_add_count* into a $floor\_value$ and a $fractional\_part$
    if $floor\_value > 0$ **then**
      Add $floor\_value$ number of nodes
    end if
    if $fractional\_part > 0$ & $rand \in [0,1) < fractional\_part$ **then**
      Add an additional node
    end if
    for each node in g **do**
      Generate a random number $rand \in [0,1)$
      if the node is Susceptible and $rand < \beta_1 * I/N$ **then**
        Change the status to Exposed
      else if the node is Exposed and $rand < \beta_2$ **then**
        Change the status to Infected
      else if the node is Infected **then**
        Generate another random number *rand*2
        if $rand < \beta_3$ **then**
          Change the status to Recovered
        end if
        if $rand2 < \alpha_1$ **then**
          Change the status to Treatment
        end if
      else if the node is under Treatment and $rand < \alpha_2$ **then**
        Change the status to Recovered
      end if
    end for
    Count and store the number of nodes in *S_count*, *E_count*, *I_count*, *T_count*, *R_count*, *N_count*
    Calculate and store metrics in *degree_dist*, *clustering_coeff*, *avg_path_length*, *largest_comp_size*
    Store the experiment result
  end for
  Calculate and store the averages of num_exp experiments
end for
return averages

[1] For Erdos–Rényi networks, *n_par*1 represents the probability p. For Barabási–Albert networks, *n_par*1 is multiplied by n and used as the m parameter, which determines the number of edges to attach from a new node to existing nodes. For Watts–Strogatz networks, *n_par*1 represents the rewiring probability p.

[2] This parameter is utilized only for Watts–Strogatz networks, where *n_par*2 represents the k parameter, indicating the number of nearest neighbors each node is initially connected to. It is not used for Erdos–Rényi or Barabási–Albert networks.

Our network based approach scans connections of each individual based on edges of graph g (Alg 1, line 2) and changes their state during each simulation time step according to specific rules and probabilities (Alg 1, steps 24-41). These rules capture the disease transmission process and the recovery process. The transition probabilities for status changes are determined by a set of parameters, which we introduced in Sect. 2.1 for the homogeneous model. The disease transmission process includes the following transitions:

- Susceptible individuals can become exposed if they interact with infected or exposed individuals.
- Exposed individuals can become infected.
- Infected individuals can either go into treatment or recover.
- Individuals in treatment can recover.
- Recovered individuals remain in the recovered state for the complete cycle.

In addition to these transitions, individuals can also enter or leave the population due to recruitment and death rates. New susceptible individuals can enter the population at a constant (recruitment) rate (Λ), and individuals can leave the population due to natural death (μ) or disease-induced deaths (δ_I) and (δ_T). New individuals are connected to the existing network by adding edges to the newly created node. In this step, we considered the network type for adding edges to keep the structure intact through time. The specific procedures for node addition are outlined below.

- **Erdős–Rényi Network**: When adding new nodes to an Erdős–Rényi network, nodes are attached to the existing network through a random selection process. In the code, after incrementing the node counter, a new node is added with the status "S" (susceptible) and labeled according to the current node counter. Then, a number of existing nodes are randomly chosen to connect to the new node. The number of nodes selected for attachment is determined by the parameter 'p', which defines the connection probability. These edges are added to the graph as long as there is no self-loop. This random attachment process mimics the structure of Erdős–Rényi networks, where the edges between nodes are established randomly.
- **Barabási–Albert Network**: In a Barabási–Albert network, new nodes are added according to the preferential attachment mechanism. When a new node is added, it is connected to existing nodes based on their degree. The probability of attaching a new node to an existing node is proportional to the degree of the existing node, meaning nodes with higher degrees (more connections) are more likely to receive new edges. The code accomplishes this by first calculating the degree of all nodes and then using these degrees to determine the likelihood of selecting each node for attachment. The number of edges to be added is determined by the mean degree of the existing network. This preferential attachment mechanism results in a scale-free network, where some nodes become highly connected (hubs) while most nodes have relatively few connections.
- **Watts–Strogatz Network**: For the Watts–Strogatz network, the addition of new nodes is somewhat more structured, reflecting the small-world properties of the network. Initially, the new node is connected to the 'k' nearest neighbors based on shortest path calculations. This ensures that the local neighborhood structure of the network is preserved. Once the new node is connected to its nearest neighbors, the edges are rewired with a probability 'p'. In the code, this rewiring process involves checking if an edge should be replaced based on a random number generation. If the condition is met, an existing neighbor of the new node is replaced with another node from the network, chosen randomly but ensuring that it is not already a neighbor of the new node. This rewiring simulates the transition from a regular lattice to a small-world network, where the network retains a high degree of clustering but also has long-range connections that facilitate faster spreading of the infection. These mechanisms for node addition are designed to reflect the fundamental topological properties of the respective network models, ensuring that each network evolves according to its characteristic structure. Using these methods, we can observe how the topology of the network affects the disease dynamics and better understand the interplay between network structure and the spread of infection.

Nodes removed due to natural death are selected randomly from the complete network, the nodes removed due to infection are selected randomly from nodes with infected status and the nodes removed during treatment are selected randomly from nodes with treatment status. Individuals in the infected state can transition to the treatment state, and those in the treatment state can eventually recover. This aspect of the model allows us to explore the effects of interventions such as medical treatment or quarantine on the course of the outbreak. Adjusting the treatment-related parameters, we can simulate scenarios with varying intervention levels and observe their effects on disease spread.

The state of the population is recorded at each time step, including the number of individuals in each state and the total population size. The number of individuals in each state is plotted over time for each run, allowing for a comparison of the disease dynamics across different runs. These experiments provide a detailed and flexible framework for simulating and analyzing disease outbreaks in a population. By adjusting the parameters and initial conditions, it can be used to study a wide range of diseases and outbreak scenarios. An important note here is that when adding new members to the networks (Algorithm 1, steps 16–23), we alter the edge addition method according to the network types.

Representing the population as a graph enables the incorporation of complex interaction patterns and population heterogeneity, enabling the study of disease spread in real-world scenarios. Due to the stochastic nature of the graph generation, initial conditions, and the disease transmission process, simulation results vary between runs. Thus, we run multiple simulations and find the average population dynamic curves, which we use to compare with the homogeneous model (Eq. 1). Each experiment represents a unique combination of network topology and model parameters, providing an understanding of disease dynamics under various conditions.

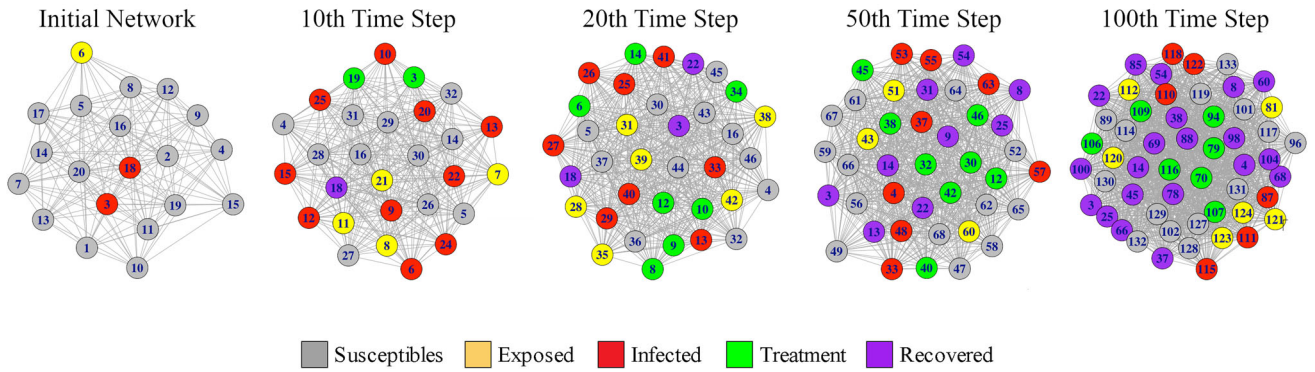

Fig. 2 Illustration of status changes of nodes over time for an Erdős–Rényi graph with$p = 0.9$ and n = 20 according to our network *SEITR* model with viral parameters $\Lambda = 1.1$, $\beta_1 = 0.8$, $\beta_2 = 0.18$, $\beta_3 = 0.02$, $\alpha_1 = 0.1$, $\alpha_2 = 0.055$, $\delta_I = 0.03$, $\delta_T = 0.03$, and $\mu = 0.01$. The nodes are colored according to their status. The initial network (left) shows that there are 17 susceptible, 1 exposed, and 2 infected nodes in the graph, consisting of 20 nodes named from 1 to 20. As the network evolves, new members join (birth) and some leave (death), resulting in varying nodes at each time step, ultimately reaching a total of 133 nodes-indicating 113 new additions over 100 time steps. The progression illustrates how an infection spreads through a network and how interventions can help control the spread and eventually eradicate the infection

3 Results

3.1 SEITR model analysis for an Erdős–Rényi network

To illustrate the network-based SEITR algorithm, we first simulate the dynamic evolution of states on a small Erdős–Rényi network with $n = 20$ nodes (Fig. 2). The simulation begins with an initial configuration of susceptible, exposed, infected, treated, and recovered individuals. As the simulation progresses, we observe that the infection spreads across the network, with more nodes transitioning through different states. Initially, many nodes remain susceptible, but as time progresses, more nodes become exposed and infected. By the 10th time step, several nodes, including nodes 3 and 19, have transitioned to the treated state, and node 18 has recovered, suggesting that intervention measures (e.g., treatment) or natural recovery processes are beginning to attenuate the infection. The number of treated and recovered nodes continues to rise between the 10th and 20th time steps, while a few nodes remain in the susceptible, exposed, or infectious states. By the 50th time step, the spread of the infection has been significantly controlled, with most nodes either treated or recovered, and very few nodes still infectious or exposed. This indicates that the interventions and natural recovery processes are effectively curbing the infection. By the 100th time step, nearly all nodes have recovered, and only a small number remain in the treated state, signaling the near eradication of the infection across the network.

To further illustrate the SEITR model's dynamics, we conduct the experiment on an Erdős–Rényi graph with more nodes ($n = 100$) (Fig. 3). For this experiment, the initial conditions are 70 susceptible, 10 infected, and 20 exposed individuals. The network is generated with a high probability of edge creation ($p = 0.85$), ensuring a high degree of connectivity within the graph. The status transitions of nodes are stored for all time steps, and the results were compared with the numerical solution of the corresponding system of ordinary differential equations (ODEs) given by Eq. 1. The simulation results and the ODE solutions show a high degree of correspondence across all five statuses (Fig. 3). This simulation shows that the SEITR network model with a high-connectivity random graph can accurately capture the dynamics of disease transmission and control strategies for the corresponding homogeneous model.

These experiments model a scenario, such as a farmstead, where each individual is equally likely to interact with others, and the random graph structure ensures that all nodes have a chance to influence each other. The highly connected nature of this network facilitates smooth transitions between the states of the nodes, but in real-world networks, such connectivity may not always be present. The random graph scenario provides a useful baseline calibration, but it is important to consider how different network structures could affect disease dynamics and intervention strategies in more realistic settings.

3.2 SEITR model analysis for multiple network types

To characterize the effect of network structure on disease dynamics, we apply the SEITR model to three distinct types of networks: Erdős–Rényi, Barabási–Albert, and Watts–Strogatz. We use a range of parameters and sizes for each network. For Erdős–Rényi networks, we generate graphs with probability 'p' set to 0.2, 0.5, and 0.9. For Barabási–Albert networks, we use 'm' set to $n * 0.2$, $n * 0.5$, and $n * 0.9$, which provide similar connection probabilities to Erdős–Rényi networks. For Watts–Strogatz networks, we created graphs with k set to 5, 10, 20, and p set to 0.2, 0.5, 0.9, where 'k' represents the number of neighbors in the lattice and 'p' is the rewiring probability. For these combinations of parameters, we use three different network sizes: 100, 200, and 1000 nodes. This variation in network size enables us to evaluate the scalability of the model and the impact of the size of a network on experimental outcomes.

Table 1 Experiment results; normalized root mean squared deviation (NRMSD) and performance metrics across network configurations. This table presents the NRMSD values for each compartment of the SEITR model (Susceptible (S), Exposed (E), Infected (I), Treatment (T), Recovered (R)), along with the average NRMSD and performance time (in seconds) across 45 experiments conducted on three network types: Erdős–Rényi, Barabási–Albert, and Watts–Strogatz. Each configuration varies in parameters such as network size (n), connectivity probabilities (p), or degree distribution (m or k). The experiments were conducted under fixed parameter values: $\Lambda = 1.1$, $\beta_1 = 0.8$, $\beta_2 = 0.3$, $\beta_3 = 0.02$, $\alpha_1 = 0.1$, $\alpha_2 = 0.055$, $\delta_1 = 0.03$, $\delta_T = 0.03$, $\mu = 0.01$. Performance metrics indicate computational time required for each simulation. This data provides insights into the accuracy and efficiency of the SEITR model under diverse network structures and configurations

		S	E	I	T	R	Avg. Norm. RMSD	Performance (sec)
Erdős–Rényi	n = 100, $p = 0.2$	0.073	0.039	0.044	0.018	0.032	0.041	6.18
	n = 100, $p = 0.5$	0.075	0.040	0.047	0.017	0.023	0.038	7.86
	n = 100, $p = 0.9$	0.074	0.041	0.045	0.017	0.032	0.038	10.54
	n = 200, $p = 0.2$	0.075	0.040	0.047	0.017	0.027	0.038	14.04
	n = 200, $p = 0.5$	0.075	0.041	0.045	0.021	0.026	0.038	26.68
	n = 200, $p = 0.9$	0.077	0.039	0.047	0.020	0.026	0.038	52.35
	n = 1000, $p = 0.2$	0.071	0.037	0.050	0.018	0.033	0.038	1152.72
	n = 1000, $p = 0.5$	0.071	0.039	0.047	0.020	0.036	0.039	8250.61
	n = 1000, $p = 0.9$	0.071	0.038	0.048	0.019	0.032	0.038	32383.76
Barabási–Albert	n = 100, m = n*0.2	0.070	0.040	0.049	0.017	0.026	0.036	6.89
	n = 100, m = n*0.5	0.077	0.045	0.043	0.020	0.029	0.040	9.18
	n = 100, m = n*0.9	0.075	0.042	0.046	0.018	0.032	0.039	10.49
	n = 200, m = n*0.2	0.073	0.041	0.046	0.018	0.027	0.038	19.05
	n = 200, m = n*0.5	0.072	0.042	0.043	0.019	0.030	0.038	39.95
	n = 200, m = n*0.9	0.074	0.038	0.045	0.019	0.030	0.037	56.15
	n = 1000, m = n*0.2	0.071	0.037	0.048	0.018	0.033	0.038	4466.57
	n = 1000, m = n*0.5	0.071	0.037	0.048	0.018	0.032	0.037	24123.14
	n = 1000, m = n*0.9	0.069	0.037	0.049	0.019	0.033	0.038	42206.04
Watts–Strogatz	n = 100, k = 5, $p = 0.2$	0.207	0.042	0.057	0.029	0.071	0.076	6.76
	n = 100, k = 5, $p = 0.5$	0.202	0.038	0.058	0.024	0.079	0.074	6.68
	n = 100, k = 5, $p = 0.9$	0.154	0.042	0.051	0.020	0.051	0.061	6.82
	n = 100, k = 10, $p = 0.2$	0.135	0.040	0.052	0.022	0.049	0.054	6.74
	n = 100, k = 10, $p = 0.5$	0.087	0.036	0.047	0.015	0.034	0.041	6.71
	n = 100, k = 10, $p = 0.9$	0.065	0.036	0.044	0.014	0.037	0.035	6.29
	n = 100, k = 20, $p = 0.2$	0.084	0.039	0.047	0.015	0.036	0.039	6.35
	n = 100, k = 20, $p = 0.5$	0.073	0.037	0.044	0.017	0.027	0.037	6.61
	n = 100, k = 20, $p = 0.9$	0.075	0.042	0.046	0.020	0.024	0.037	7.26
	n = 200, k = 5, $p = 0.2$	0.195	0.044	0.053	0.027	0.066	0.073	11.74
	n = 200, k = 5, $p = 0.5$	0.193	0.042	0.053	0.026	0.072	0.072	11.89
	n = 200, k = 5, $p = 0.9$	0.140	0.034	0.046	0.017	0.051	0.056	12.02
	n = 200, k = 10, $p = 0.2$	0.117	0.041	0.051	0.020	0.038	0.049	11.45
	n = 200, k = 10, $p = 0.5$	0.087	0.036	0.046	0.016	0.038	0.040	11.29
	n = 200, k = 10, $p = 0.9$	0.069	0.036	0.049	0.014	0.023	0.035	11.64
	n = 200, k = 20, $p = 0.2$	0.084	0.037	0.048	0.014	0.039	0.039	11.73
	n = 200, k = 20, $p = 0.5$	0.066	0.037	0.044	0.015	0.025	0.034	12.23
	n = 200, k = 20, $p = 0.9$	0.076	0.043	0.043	0.021	0.025	0.038	13.87
	n = 1000, k = 5, $p = 0.2$	0.192	0.040	0.058	0.022	0.073	0.071	77.01
	n = 1000, k = 5, $p = 0.5$	0.163	0.038	0.056	0.017	0.069	0.062	78.16
	n = 1000, k = 5, $p = 0.9$	0.124	0.034	0.052	0.012	0.062	0.051	78.74
	n = 1000, k = 10, $p = 0.2$	0.135	0.038	0.054	0.018	0.052	0.053	77.03
	n = 1000, k = 10, $p = 0.5$	0.084	0.033	0.050	0.012	0.043	0.039	80.97
	n = 1000, k = 10, $p = 0.9$	0.063	0.034	0.048	0.014	0.036	0.035	84.42
	n = 1000, k = 20, $p = 0.2$	0.082	0.035	0.052	0.014	0.040	0.039	85.71
	n = 1000, k = 20, $p = 0.5$	0.064	0.035	0.049	0.015	0.033	0.036	100.28
	n = 1000, k = 20, $p = 0.9$	0.067	0.035	0.049	0.016	0.028	0.036	117.76

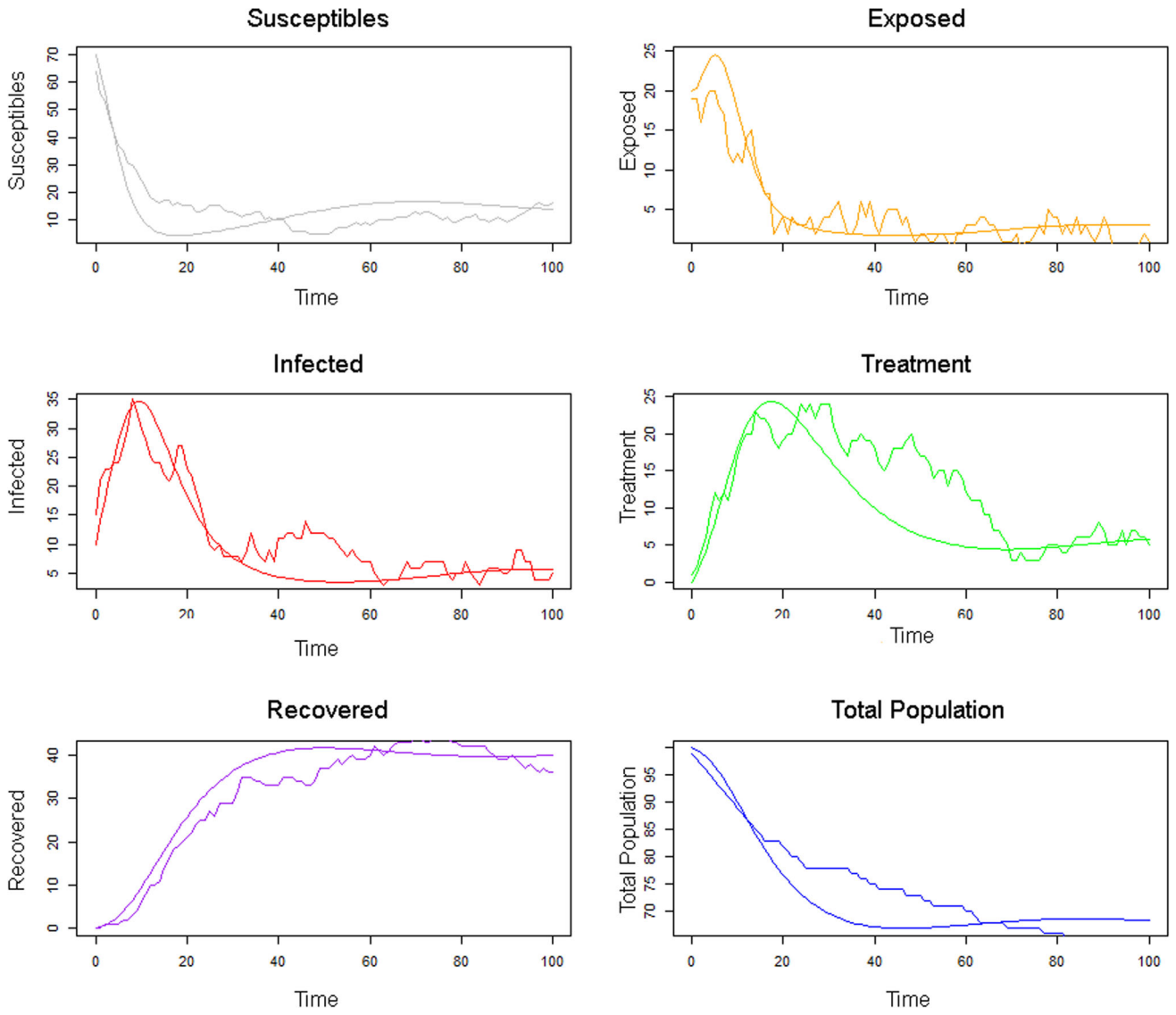

Fig. 3 SEITR densities for Erdős–Rényi network (n = 100, and$p = 0.85$, jagged lines) and the homogeneous ODE solutions of Eq. 1 (smooth lines). The network-based densities show good agreement with the homogeneous ODE model for an ER network, which has uniform connection probability. The viral parameters are, $\Lambda = 1$, $\beta_1 = 0.8$, $\beta_2 = 0.3$, $\beta_3 = 0.02$, $\alpha_1 = 0.1$, $\alpha_2 = 0.055$, $\delta_I = 0.03$, $\delta_T = 0.03$, *and* $\mu = 0.01$

All virus parameters used in the experiments are the same as in Fig. 1, and Λ is set to $n * \mu$ to ensure equal natural birth and death rates. Due to the inclusion of death through infection, we expect a slowly decreasing total population for this set of parameters. In terms of network evolution during the simulation, node removal occurs when an individual dies due to natural causes or due to infection, reducing the overall network size. Furthermore, new nodes are added during the simulation, and the manner in which new nodes are introduced varies depending on the network type.

We run 20 repetitions of each simulation for every network configuration so that noise could be mitigated in an average model of the node statuses. We compare the simulation results with the numerical solutions of the *SEITR* ODE model (Eqs.1) using the Mean Squared Deviation (MSD) to quantify the deviation of each network simulation from the homogeneous ODE solution. This quantifies network effects. To compare the different network simulations, we calculate the Root Mean Squared Deviation (RMSD) for each condition (S, E, I, T, and R). To normalize these values and adjust for the network size, we average the RMSD for each status over the five conditions (S, E, I, T, and R), and we divide the resulting average RMSD by the total number of initial nodes N for each network setup, yielding the Normalized RMSD (NRMSD). We compute the average NRMSD for each experiment by averaging the NRMSD values for the five statuses across all time steps, giving a single value to represent the overall similarity between the network simulation and the homogeneous ODE solution.

In the SEITR network experiments, the Erdős–Rényi and Barabási–Albert networks exhibit very similar agreement with the homogeneous ODE model for all network parameters, with NRMSD values typically ranging from 0.032 to 0.077 (Table 1 and

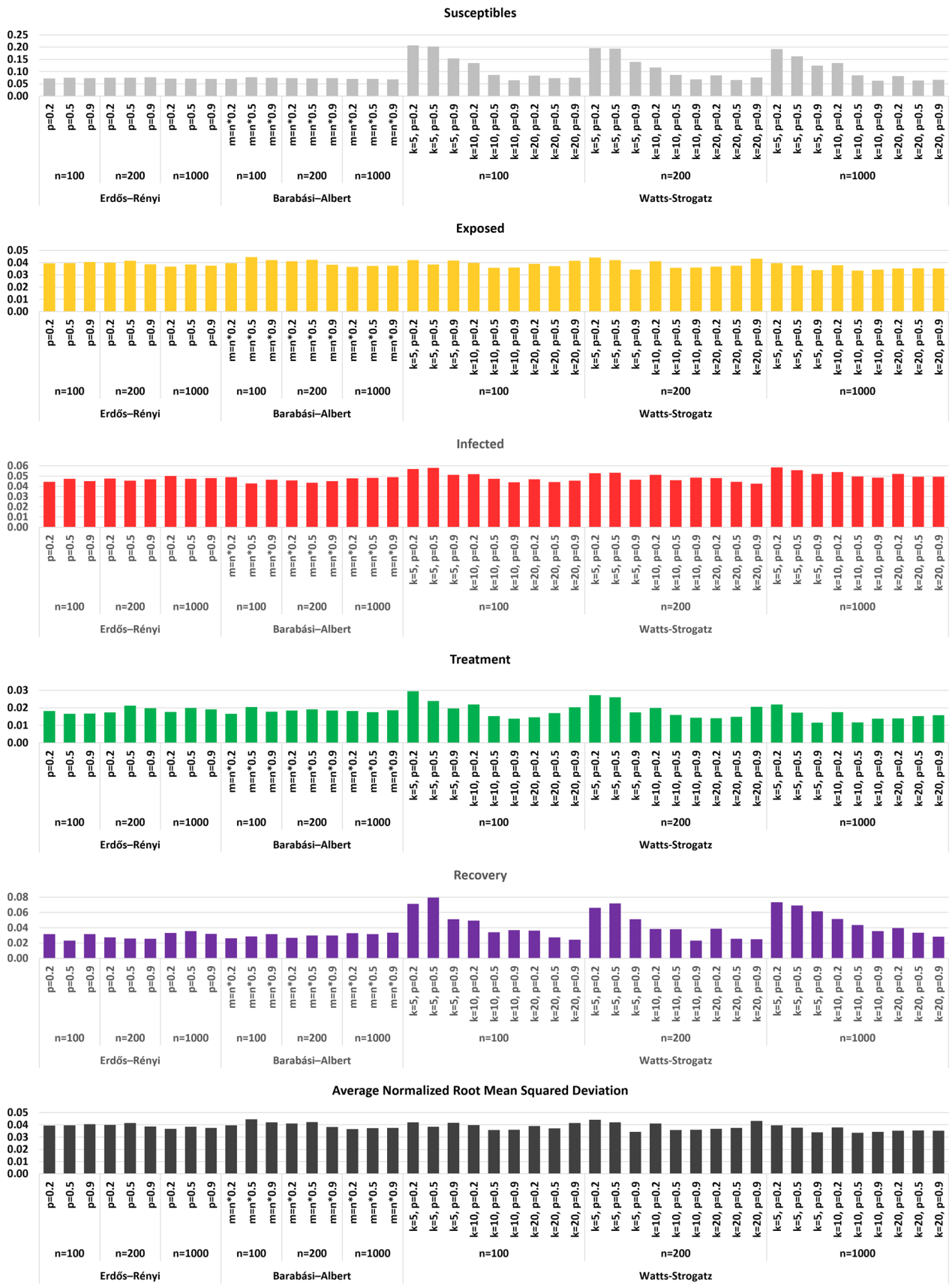

Fig. 4 Normalized root mean squared deviation (NMRSD) between network and ODE solutions for five statuses and the average NRMSD (black) for combinations of network configurations (see Table 1 caption). The Watts–Strogatz (WS) network shows the greatest deviation from a homogeneous ODE solution

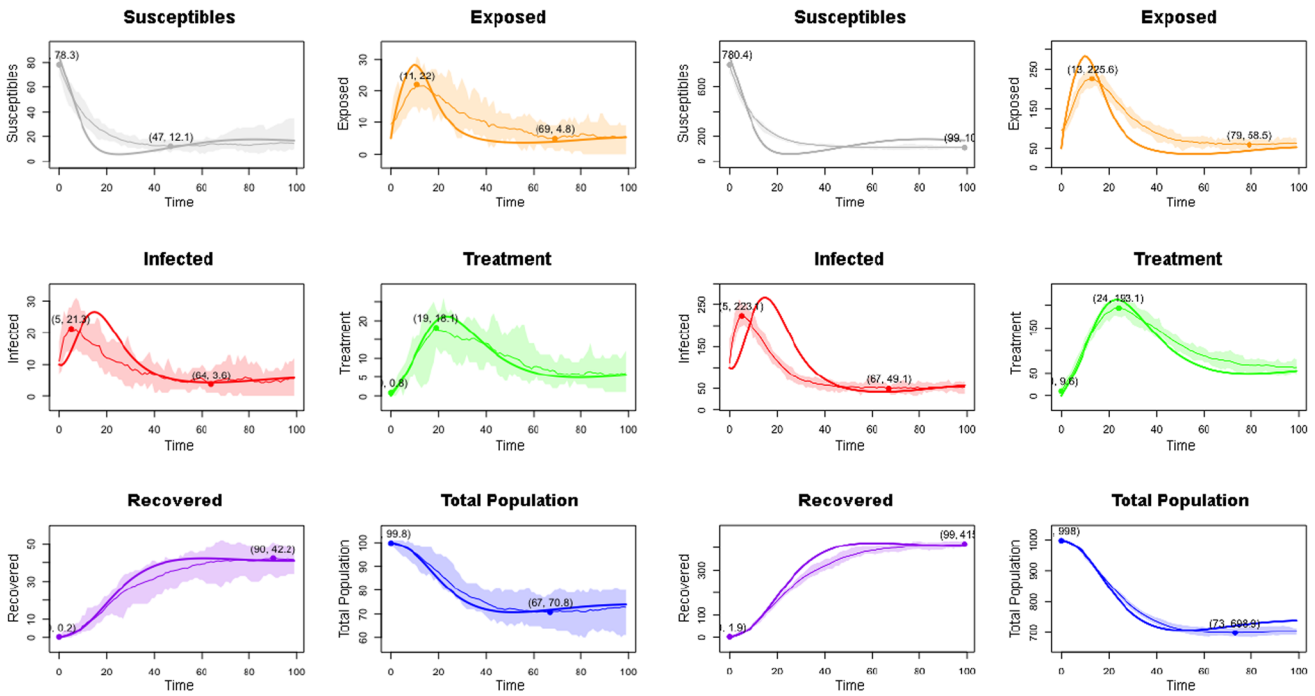

(a) Erdős-Rényi networks, n=100 and p=0.2 (b) Erdős-Rényi networks, n=1000 and p=0.2

Fig. 5 Comparison of ODE solutions and network simulations for Erdős–Rényi networks. Each subgraph (left and right) presents the dynamics of six compartments (Susceptibles, Exposed, Infected, Treatment, Recovery, and total population), contrasting ODE results (smooth lines) with averages from 20 network simulations (jagged lines bordered by shaded regions). Key differences emerge between the two network sizes: in the smaller network, epidemic peaks (E at $t = 11$, I at $t = 15$) occur earlier and with lower magnitudes compared to the larger network (E at $t = 16$, I at $t = 24$). Susceptibles decline faster and recover earlier in the smaller network, while Treatment and Recovery are more sustained in the larger network, reflecting the impact of increased size and connectivity. Total population remains stable throughout, validating the model consistency. This comparison highlights how network size shapes the timing and magnitude of epidemic dynamics

Fig. 4). This indicates that for both random and scale-free networks, the SEITR model effectively captures disease dynamics, with minimal deviation from the ODE model, regardless of the network size. Deviations from the homogeneous model is most significant for the Watts–Strogatz networks. While the Erdős–Rényi and Barabási–Albert networks are similar across network parameters, the Watts–Strogatz networks demonstrate more sensitivity to changes in parameters such as the number of neighbors k and rewiring probability p, particularly at larger network sizes (Fig. 4). These results highlight the complexity introduced by the small-world property of the Watts–Strogatz model, which can lead to more heterogeneous disease dynamics compared to random or scale-free networks. Despite these variations, all networks show the ability to capture realistic SEITR disease dynamics.

For networks with 100 nodes, the NRMSD values are particularly stable, with the highest NRMSD value for susceptible nodes at 0.073 (for $p = 0.2$, Fig. 5a) and the lowest for recovered nodes at 0.017 (for $p = 0.9$). As the network size increases to 200 nodes, the NRMSD values show a slight increase in treatment and slight decrease in recovered statuses. However, even with these shifts, the NMRSD remains quite low. For the largest network size of 1000 nodes, the NRMSD values are largely consistent with the smaller networks, with the highest NRMSD of 0.071 observed in the susceptible nodes at $p = 0.2$ (Fig. 5b). This shows, even with larger networks, the SEITR model‘s predictions are still very close to the ODE solutions, indicating that the model is scalable and reliable across different network sizes. The results for the Erdős–Rényi networks demonstrate that changes in both the connection probability p and network size have a minimal effect on the overall disease dynamics.

For networks with 100 nodes, the NRMSD values range from 0.017 to 0.077 (Table 1), with the smallest deviation observed in the recovered nodes (0.017 for $m = n * 0.2$, Fig. 6a) and the largest in the susceptible nodes (0.077 for $m = n * 0.5$ (Fig. 6b)). As the network size increases to 200 and 1000 nodes, the NRMSD values remain consistent. The results for the Barabási–Albert networks were very similar to those observed in the Erdős–Rényi networks, with minimal variation in NRMSD values. The consistency of the results across different network sizes and configurations highlights the model’s reliability in capturing disease dynamics in Barabási–Albert networks as well as Erdős–Rényi networks.

Watts–Strogatz network SEITR models, particularly when $k = 5$, have a higher deviation from the ODE model. This was observed across all rewiring probabilities ($p = 0.2$, $p = 0.5$, and $p = 0.9$), but the most significant discrepancies were found in the Susceptible, Treatment, and Recovery states. For example, in the $n = 100$ network with $k = 5$ and $p = 0.2$ (Fig. 7a), the NRMSD for Susceptible is 0.207, Treatment was 0.071, and Recovery was 0.071. These values are much higher compared to the

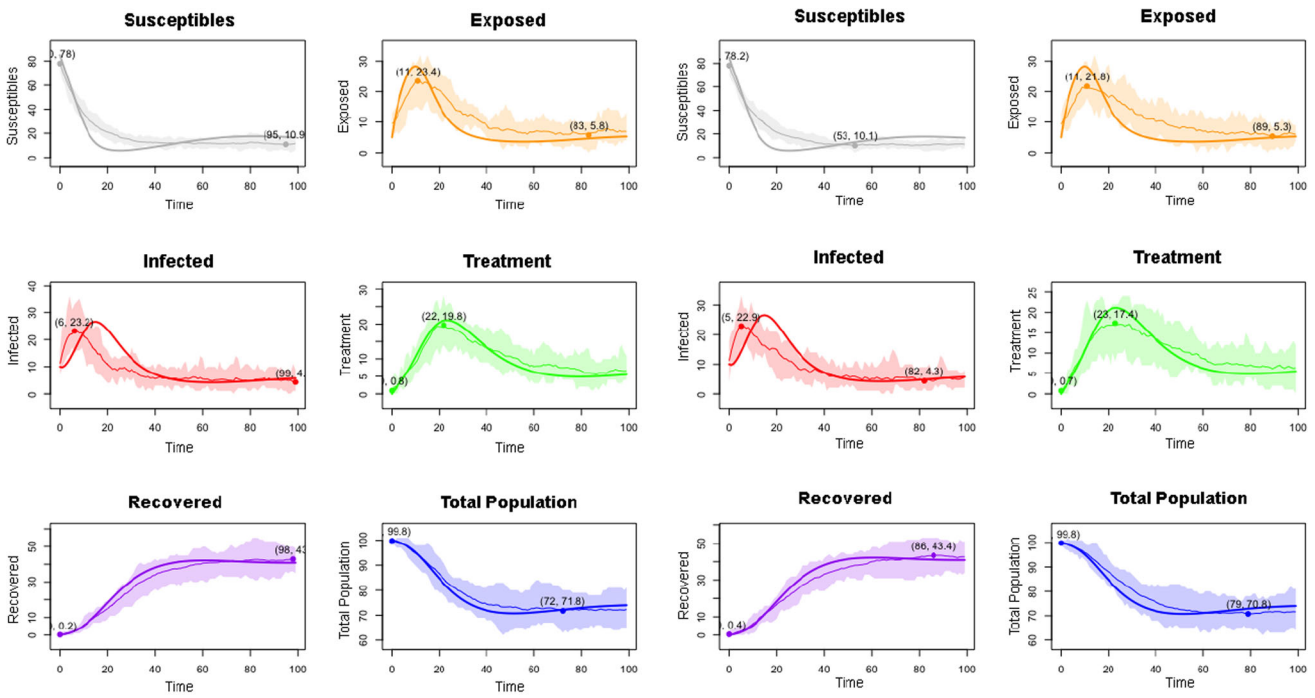

(a) Barabási-Albert networks, n=100 and m=n*0.2 (b) Barabási-Albert networks, n=100 and m=n*0.5

Fig. 6 Comparison of SEITR dynamics between two Barabási–Albert network configurations. Each subfigure (left and right) contains six plots illustrating the average behavior of Susceptibles, Exposed, Infected, Treatment, Recovered, and Total Population across 20 network simulations (jagged lines) compared to the ODE solution (smooth lines). While the overall dynamics are consistent, key differences include the timing of extreme points: in (a), Susceptibles have a dip at the 95th timestep, whereas in (b), the dip occurs earlier at the 53rd timestep. The Infected compartment reaches its peak earlier (23.2 at $t = 6$ in (a) and 22.9 at $t = 5$ in (b)) and with a lower magnitude compared to the ODE solution for both networks. The peak of the Treatment compartment is higher in (a) (19.8 at $t = 22$) compared to (b) (17.4 at $t = 23$). Other compartments exhibit similar trends across the two network configurations

corresponding Erdős–Rényi and Barabási–Albert results, where the NRMSD for Susceptible was 0.073 (Erdős–Rényi) and 0.070 (Barabási–Albert) for similar network sizes (Table 1). The high NRMSD values indicate that low connectivity (due to low k) results in disease dynamics that are more chaotic and less predictable, leading to higher deviation from the homogeneous model. This suggests that for lower k, the Watts–Strogatz network leads to disease spread that behaves less like a well-mixed (homogeneous) system. Increasing k to 10 and 20 results in lower NRMSD values for all states, bringing the results closer to the ODE solution. Across different network sizes, the Watts–Strogatz model shows a pattern where smaller networks (e.g., $n = 100$) exhibit larger NRMSD values, particularly with lower k values. For instance, in the $n = 100$ network with $k = 5$ and $p = 0.2$, the NRMSD for Susceptible was 0.207, while for $n = 1000$ with the same parameters (Fig. 7b), the NRMSD for Susceptible was lower, at 0.192. This suggests that as the network size increases, the impact of small-world network properties, such as clustering and rewiring, becomes more distributed, which leads to dynamics that are closer to the homogeneous ODE model.

3.3 SEITR model simulation performance

In this section, we compare the performance of the SEITR model across different network types by evaluating the runtime for each experiment setup. Since runtime is a crucial factor in assessing the scalability and efficiency of the model, this comparison provides insights into how different network types and their parameters affect computational performance. For the Erdős–Rényi network, runtime increases substantially as both the network size n and connection probability p rise. The randomness in edge connections in Erdős–Rényi networks results in larger sample spaces for edge selection as the network becomes denser. For example, at $n = 1000$, the runtime ranges from 1,152.72 s (for $p = 0.2$) to 32,383.76 s (for $p = 0.9$), with larger values of p leading to a denser network and more expensive computations. The combination of a larger network and higher connectivity makes the Erdős–Rényi network particularly sensitive to these parameters, resulting in a sharp increase in runtime (Fig. 8).

The Barabási–Albert network follows a similar pattern, where increases in both network size and the number of edges per new node m lead to higher runtimes. At $n = 1000$, the runtime spans from 4,466.57 s (for $m = n * 0.2$) to 42,206.04 s (for $m = n * 0.9$). The preferential attachment mechanism in Barabási–Albert networks, where nodes preferentially connect to others with higher

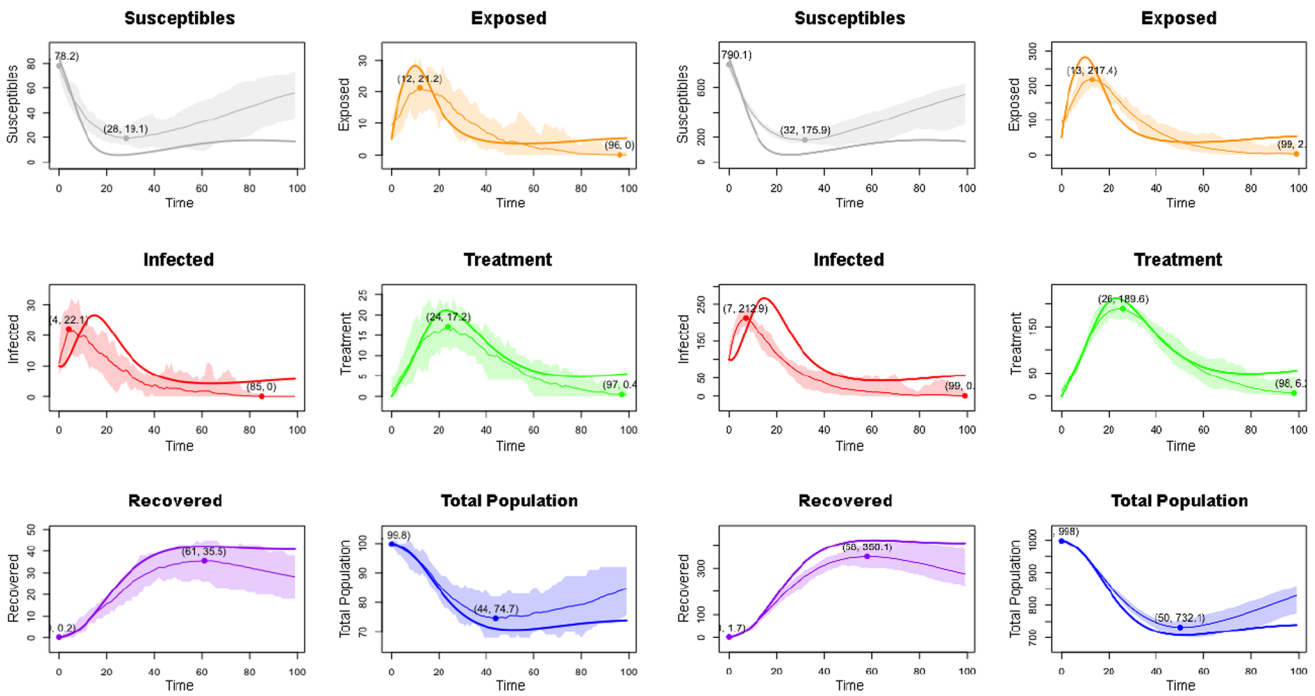

(a) Watts-Strogatz networks, n=100, k=5 and p=0.2

(b) Watts-Strogatz networks, n=1000, k=5 and p=0.2

Fig. 7 Comparison of SEITR dynamics between network simulation averages and ODE solutions for Watts–Strogatz networks. Despite a slightly higher NRMSD compared to the Erdos–Renyi and Barabasi-Albert networks (see Fig. 4), Watts–Strogatz networks still achieve strong alignment with the ODE models. In the Susceptible compartment, the network simulation sharply diverges from the ODE solution after reaching its minimum, with the population remaining significantly higher in the network model. This suggests that the small-world structure of the Watts–Strogatz network slows down the depletion of susceptibles, likely due to localized clustering and limited long-range transmission. Subfigure**a** shows greater variability in the susceptible and treatment compartments, reflecting structural irregularities inherent in smaller Watts–Strogatz networks. The treatment compartment peaks at approximately 24.1 at $t = 17$, similar to subfigure **b** but with a marginally sharper peak and quicker decline. In subfigure **b**, a larger population dampens discrepancies, yielding smoother curves and a later peak in treatment (around $t = 18$). While Watts–Strogatz networks exhibit slightly increased deviations due to their clustering and rewiring characteristics, they validate the robustness of simulations in approximating ODE models for larger-scale systems

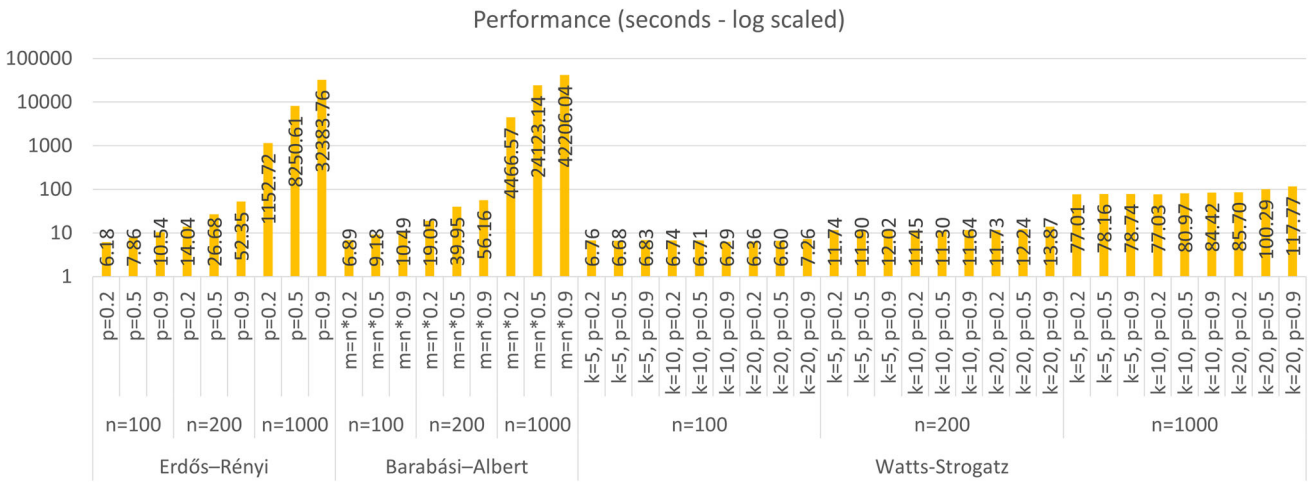

Fig. 8 Computational performance metrics of SEITR simulations across experiments. Bars are the CPU time (in seconds) on log scale for SEITR model simulations for 45 experiment configurations, as listed in Table 1. Individual experiment sets (x-axis) are grouped by network types (Erdős–Rényi, Barabási–Albert, and Watts–Strogatz). The logarithmic scale highlights the substantial differences in simulation times, particularly for larger network sizes (n) and higher connectivity parameters (p, m, or k)

degrees, results in a more complex degree distribution. This mechanism requires additional computational resources, particularly as m increases, leading to a higher processing time due to the increased complexity of the network structure.

Watts–Strogatz network, in contrast, shows a more stable runtime across different values of the parameters k (the number of neighbors) and p (the rewiring probability). The rewiring process and the localized connection structure of Watts–Strogatz networks do not significantly affect runtime, and the results indicate no major differences when varying k or p. However, network size still influences runtime, though the effect is not as drastic as in Erdős–Rényi or Barabási–Albert networks. At $n = 1000$, the runtime remains relatively stable across different settings for k and p, with slight increases observed as the network size grows. This suggests that while the Watts–Strogatz network's localized structure is less computationally demanding compared to the more globally connected Erdős–Rényi and Barabási–Albert networks, the network size still plays a role in increasing runtime, albeit more gradually.

The differences in performance across these network types can be attributed to the underlying mechanisms governing edge formation. In both Erdős–Rényi and Barabási–Albert networks, the combination of larger networks and increased connectivity or attachment results in higher computational costs, with Erdős–Rényi networks being particularly sensitive to the connection probability p, and Barabási–Albert networks being influenced by the degree distribution affected by m. In contrast, the Watts–Strogatz network's localized structure allows for more stable performance across varying parameters, with network size remaining the primary factor influencing runtime.

4 Conclusions and future work

In this study, we investigated the dynamics of disease spread across different network structures, specifically Erdős–Rényi, Barabási–Albert, and Watts–Strogatz networks. We simulated *SEITR* disease dynamics on these networks under various conditions. As the network degree distributions became more uniform, the disease dynamics agreed with the expected trends of a homogeneous ODE solution. We also observed that certain network topologies led to deviations from the homogeneous model disease dynamics. Moreover, the experiments highlighted the stochastic nature of disease spread. By running multiple iterations of the experiments, a range of outcomes was observed, reflecting the inherent randomness in disease transmission and network generation. Our results demonstrated the ability of the SEITR network simulation to accurately replicate homogeneous ODE results while accounting for stochastic variations inherent to network-based simulations. Key epidemiological metrics, such as the timing of infection peaks, susceptible dips, and recovery plateaus, were consistently aligned with expectations across network types, validating the model's applicability to various scenarios. Overall, the combination of network theory and epidemiological modeling provides a flexible and insightful framework for studying disease dynamics.

Our *SEITR* network algorithm also includes realistic disease transmission and dynamic parameters that one would use in ODE models. By adjusting these parameters, the model can be tailored to simulate a wide range of diseases and outbreak scenarios, enhancing its versatility and applicability. Further, the experiments demonstrated the impact of various parameters on disease dynamics, such as the rate of new individuals entering the population (Λ), the probabilities of transitioning between states (β_1, β_2, β_3, α_1, α_2), and the rates of disease-induced death (δ_I, δ_T). These experiments underscore the importance of network structure and size in epidemiological modeling and contribute to our understanding of disease dynamics. The findings can inform strategies for disease control and prevention.

This study opens several avenues for future exploration. In this study, we utilized Erdős–Rényi, Barabási–Albert, and Watts–Strogatz network graphs to simulate a cattle population. While these network structures capture certain aspects of real-world populations, they offer a simplified representation. Future research could focus on exploring more intricate network models that better encapsulate the diversity and complexity of real-world population structures. For instance, networks incorporating hierarchical or multilayered structures, such as multiplex networks or temporal networks, could be utilized to represent populations where interactions are influenced by overlapping social, spatial, or temporal factors. Such models could provide deeper insights into disease dynamics, particularly in settings where interactions are context-dependent or evolve over time. Future research could incorporate network graphs based on empirical data representing actual populations, such as those of a county, state, or entire country. This adaptation would enhance the model's applicability to policy-making and public health planning. However, such an approach would require significant computational resources due to the complexity and scale of real-world networks.

Another promising direction is the introduction of time-dependent treatment interventions. In the current model, treatment availability was assumed to begin at the first step of the simulation. Future implementations could parameterize treatment initiation to occur at a specific time step, allowing for the examination of delayed or phased treatment strategies and their impact on epidemic outcomes. This extension would provide more realistic insights into scenarios where treatment resources are mobilized at different stages of an outbreak. Furthermore, incorporating additional factors, such as spatial heterogeneity, mobility patterns, or vaccination strategies, could further extend the model's relevance to practical epidemiological applications. These enhancements would continue to bridge the gap between theoretical modeling and real-world scenarios.

The SEITR network model could also be refined to incorporate additional realistic elements, such as age structure. Age can significantly influence an individual‘s susceptibility to infection, their likelihood of transmitting the disease, and their probability of recovery. Another potential enhancement is to include spatial structure in the model, as the spatial distribution of individuals can greatly impact disease spread. This could be achieved by using spatially explicit network models or by incorporating spatially dependent transmission rates into the model. In this study, the model parameters were set manually based on reasonable assumptions. However, in a real-world outbreak, these parameters would need to be estimated from data. Future work could explore methods for parameter estimation, such as maximum likelihood estimation or Bayesian inference. These methods could be used to fit the model to outbreak data and estimate the parameters that best explain the observed disease dynamics.

Funding There is no funding available at the moment.

Data availability statement All data supporting the findings of this study are available with references within the manuscript.

Declarations

Conflict of interest This work does not have any conflict of interest.

Declaration of generative AI and AI-assisted technologies in the writing process The authors utilized the free AI tool QuillBot to improve the manuscript's grammar. Following its use, the authors reviewed and edited the content as necessary, taking full responsibility for the final publication.

Appendix

The appendix provides a comprehensive presentation of the experimental results in full detail. This includes an extended version of the results table from the main text, which features Mean Squared Deviation (MSD), Root Mean Squared Deviation (RMSD), and total population values for all 45 experiment sets. Additionally, individual experiment graphs for each set are included to visually demonstrate the simulation outcomes. These graphs and detailed metrics showcase the performance and accuracy of the network-based SEITR model across various configurations, including Erdős–Rényi, Barabási–Albert, and Watts–Strogatz networks of differing sizes and connectivities (Table 2).

Table 2 Extended experiment results: comprehensive metrics and insights from SEITR Model experiments across network configurations. This table presents detailed metrics, including mean squared deviation (MSD), root mean squared deviation (RMSD), and total population over time for 45 experiments conducted using the SEITR model on three network types: Erdős–Rényi, Barabási–Albert, and Watts–Strogatz. All experiments were performed on networks of three sizes: $n = 100$, $n = 200$, and $n = 1000$. For Erdős–Rényi networks, connectivity probabilities were set at $p = 0.2$, $p = 0.5$ and $p = 0.9$. Barabási–Albert networks used degree parameters $m = 0.2 * n$, $m = 0.5 * n$ and $m = 0.9 * n$. Watts–Strogatz networks were configured with neighborhood sizes $k = 5$, $k = 10$ and $k = 20$, and rewiring probabilities $p = 0.2$, $p = 0.5$ and $p = 0.9$. Simulations were performed under fixed parameter values: $\Lambda = 1.1$, $\beta_1 = 0.8$, $\beta_2 = 0.3$, $\beta_3 = 0.02$, $\alpha_1 = 0.1$, $\alpha_2 = 0.055$, $\delta_1 = 0.03$, $\delta_T = 0.03$, $\mu = 0.01$. The table highlights the influence of network structure on disease dynamics. Watts–Strogatz networks, with their balance of regularity and randomness, exhibited the largest deviations in the infectious compartments compared to the homogeneous ODE model. Barabási–Albert networks emphasized the role of hub nodes in disease spread, reflecting real-world heterogeneity, while Erdős–Rényi networks provided a baseline for random connectivity. This table reveals how network structure and parameter variations shape the dynamics of the SEITR model

	n		S			E			I			T			R			N				
			MSD	RMSD	NRMSD	MSD	RMSD	NRMSD	MSD	RMSD	NRMSD	MSD	RMSD	NRMSD	MSD	RMSD	NRMSD	MSD	RMSD	NRMSD	Avg. NRMSD	runtime
ER	100	$p = 0.2$	52.791	7.266	0.073	15.560	3.945	0.039	19.754	4.445	0.044	3.316	1.821	0.018	9.930	3.151	0.032	3.119	1.766	0.018	0.041	6.180793
	100	$p = 0.5$	56.209	7.497	0.075	15.726	3.966	0.040	22.408	4.734	0.047	2.765	1.663	0.017	5.321	2.307	0.023	5.832	2.415	0.024	0.038	7.864507
	100	$p = 0.9$	54.181	7.361	0.074	16.468	4.058	0.041	20.232	4.498	0.045	2.802	1.674	0.017	10.028	3.167	0.032	5.107	2.260	0.023	0.038	10.5411
	200	$p = 0.2$	227.203	15.073	0.075	64.016	8.001	0.040	90.094	9.492	0.047	12.111	3.480	0.017	29.847	5.463	0.027	16.522	4.065	0.020	0.038	14.0402
	200	$p = 0.5$	226.950	15.065	0.075	68.767	8.293	0.041	82.502	9.083	0.045	18.110	4.256	0.021	26.524	5.150	0.026	18.456	4.296	0.021	0.038	26.68177
	200	$p = 0.9$	236.202	15.369	0.077	59.788	7.732	0.039	87.549	9.357	0.047	15.581	3.947	0.020	26.119	5.111	0.026	13.628	3.692	0.018	0.038	52.34912
	1000	$p = 0.2$	5067.717	71.188	0.071	1353.875	36.795	0.037	2498.015	49.980	0.050	311.326	17.644	0.018	1094.436	33.082	0.033	410.833	20.269	0.020	0.038	1,152.72
	1000	$p = 0.5$	5071.580	71.215	0.071	1482.472	38.503	0.039	2244.143	47.372	0.047	398.964	19.974	0.020	1268.045	35.610	0.036	466.337	21.595	0.022	0.039	8,250.61
	1000	$p = 0.9$	5006.293	70.755	0.071	1407.783	37.520	0.038	2302.632	47.986	0.048	368.176	19.188	0.019	1028.313	32.067	0.032	445.023	21.096	0.021	0.038	32,383.76
BA	100	m = n*0.2	48.940	6.996	0.070	15.610	3.951	0.040	24.008	4.900	0.049	2.737	1.654	0.017	6.860	2.619	0.026	2.889	1.700	0.017	0.036	6.891965
	100	m = n*0.5	59.782	7.732	0.077	19.886	4.459	0.045	18.206	4.267	0.043	4.177	2.044	0.020	8.257	2.873	0.029	6.010	2.452	0.025	0.040	9.182101
	100	m = n*0.9	56.548	7.520	0.075	17.636	4.199	0.042	21.511	4.638	0.046	3.173	1.781	0.018	10.074	3.174	0.032	5.238	2.289	0.023	0.039	10.48945
	200	m = n*0.2	214.409	14.643	0.073	67.387	8.209	0.041	83.323	9.128	0.046	13.630	3.692	0.018	28.391	5.328	0.027	16.367	4.046	0.020	0.038	19.04765
	200	m = n*0.5	208.592	14.443	0.072	71.573	8.460	0.042	75.293	8.677	0.043	14.601	3.821	0.019	35.841	5.987	0.030	16.293	4.036	0.020	0.038	39.95492
	200	m = n*0.9	216.695	14.721	0.074	58.410	7.643	0.038	81.572	9.032	0.045	13.735	3.706	0.019	35.454	5.954	0.030	15.360	3.919	0.020	0.037	56.15544
	1000	m = n*0.2	4995.806	70.681	0.071	1339.869	36.604	0.037	2284.719	47.799	0.048	329.483	18.152	0.018	1078.259	32.837	0.033	437.795	20.924	0.021	0.038	4,466.57
	1000	m = n*0.5	5005.666	70.751	0.071	1386.809	37.240	0.037	2330.691	48.277	0.048	308.421	17.562	0.018	993.861	31.526	0.032	385.070	19.623	0.020	0.037	24,123.14
	1000	m = n*0.9	4696.009	68.527	0.069	1400.347	37.421	0.037	2389.884	48.886	0.049	348.420	18.666	0.019	1115.154	33.394	0.033	447.032	21.143	0.021	0.038	42206.04

Table 2 continued

	n		S			E			I			T			R			N				
			MSD	RMSD	NRMSD	MSD	RMSD	NRMSD	MSD	RMSD	NRMSD	MSD	RMSD	NRMSD	MSD	RMSD	NRMSD	MSD	RMSD	NRMSD	Avg. NRMSD	runtime
WS	100	$k = 5, p = 0.2$	429.704	20.729	0.207	17.663	4.203	0.042	32.391	5.691	0.057	8.691	2.948	0.029	50.707	7.121	0.071	26.323	5.131	0.051	0.076	6.763343
	100	$k = 10, p = 0.2$	182.503	13.509	0.135	15.832	3.979	0.040	26.864	5.183	0.052	4.804	2.192	0.022	24.313	4.931	0.049	6.288	2.508	0.025	0.054	6.742341
	100	$k = 20, p = 0.2$	69.964	8.364	0.084	15.203	3.899	0.039	22.007	4.691	0.047	2.149	1.466	0.015	13.174	3.630	0.036	2.284	1.511	0.015	0.039	6.355329
	100	$k = 5, p = 0.5$	408.077	20.201	0.202	14.743	3.840	0.038	33.627	5.799	0.058	5.723	2.392	0.024	62.954	7.934	0.079	19.312	4.395	0.044	0.074	6.683067
	100	$k = 10, p = 0.5$	75.404	8.684	0.087	12.815	3.580	0.036	22.427	4.736	0.047	2.340	1.530	0.015	11.681	3.418	0.034	5.628	2.372	0.024	0.041	6.711229
	100	$k = 20, p = 0.5$	53.228	7.296	0.073	13.744	3.707	0.037	19.461	4.411	0.044	2.872	1.695	0.017	7.444	2.728	0.027	4.675	2.162	0.022	0.037	6.600499
	100	$k = 5, p = 0.9$	236.504	15.379	0.154	17.438	4.176	0.042	26.208	5.119	0.051	3.883	1.970	0.020	26.053	5.104	0.051	22.532	4.747	0.047	0.061	6.828653
	100	$k = 10, p = 0.9$	41.778	6.464	0.065	12.965	3.601	0.036	19.212	4.383	0.044	1.915	1.384	0.014	13.498	3.674	0.037	1.701	1.304	0.013	0.035	6.293789
	100	$k = 20, p = 0.9$	56.126	7.492	0.075	17.253	4.154	0.042	20.770	4.557	0.046	4.123	2.030	0.020	5.983	2.446	0.024	2.802	1.674	0.017	0.037	7.26089
	200	$k = 5, p = 0.2$	1527.161	39.079	0.195	77.672	8.813	0.044	111.679	10.568	0.053	29.845	5.463	0.027	173.881	13.186	0.066	98.175	9.908	0.050	0.073	11.74068
	200	$k = 10, p = 0.2$	546.108	23.369	0.117	67.368	8.208	0.041	104.578	10.226	0.051	15.884	3.985	0.020	59.222	7.696	0.038	30.905	5.559	0.028	0.049	11.45313
	200	$k = 20, p = 0.2$	283.733	16.844	0.084	54.062	7.353	0.037	92.104	9.597	0.048	7.965	2.822	0.014	59.597	7.720	0.039	6.662	2.581	0.013	0.039	11.72695
	200	$k = 5, p = 0.5$	1496.755	38.688	0.193	71.068	8.430	0.042	113.222	10.641	0.053	27.147	5.210	0.026	206.929	14.385	0.072	85.743	9.260	0.046	0.072	11.89937
	200	$k = 10, p = 0.5$	300.629	17.339	0.087	51.057	7.145	0.036	84.533	9.194	0.046	10.165	3.188	0.016	58.287	7.635	0.038	15.850	3.981	0.020	0.040	11.29993
	200	$k = 20, p = 0.5$	172.469	13.133	0.066	56.064	7.488	0.037	78.702	8.871	0.044	8.875	2.979	0.015	25.962	5.095	0.025	10.249	3.201	0.016	0.034	12.23684
	200	$k = 5, p = 0.9$	783.887	27.998	0.140	46.810	6.842	0.034	86.392	9.295	0.046	12.034	3.469	0.017	104.080	10.202	0.051	10.202	8.990	0.045	0.056	12.02282
	200	$k = 10, p = 0.9$	188.770	13.739	0.069	52.006	7.212	0.036	94.226	9.707	0.049	8.270	2.876	0.014	21.256	4.610	0.023	13.212	3.635	0.018	0.035	11.6433
	200	$k = 20, p = 0.9$	230.424	15.180	0.076	74.741	8.645	0.043	72.716	8.527	0.043	17.058	4.130	0.021	24.847	4.985	0.025	21.680	4.656	0.023	0.038	13.86879
	1000	$k = 5, p = 0.2$	36942.379	192.204	0.192	1560.945	39.509	0.040	3421.499	58.494	0.058	480.635	21.923	0.022	5381.874	73.361	0.073	1558.386	39.476	0.039	0.071	77.0094
	1000	$k = 10, p = 0.2$	18131.35	134.653	0.135	1439.831	37.945	0.038	2906.524	53.912	0.054	307.954	17.549	0.018	2653.219	51.509	0.052	595.821	24.409	0.024	0.053	77.03
	1000	$k = 20, p = 0.2$	6673.321	81.690	0.082	1242.245	35.246	0.035	2715.809	52.113	0.052	193.300	13.903	0.014	1561.821	39.520	0.040	110.328	10.504	0.011	0.039	85.702
	1000	$k = 5, p = 0.5$	26549.780	162.941	0.163	1423.673	37.732	0.038	3123.451	55.888	0.056	300.466	17.334	0.017	4748.192	68.907	0.069	892.931	29.882	0.030	0.062	78.1575
	1000	$k = 10, p = 0.5$	7134.452	84.466	0.084	1118.314	33.441	0.033	2453.979	49.538	0.050	135.378	11.635	0.012	1880.859	43.369	0.043	174.586	13.213	0.013	0.039	80.96664
	1000	$k = 20, p = 0.5$	4101.439	64.042	0.064	1257.331	35.459	0.035	2436.649	49.362	0.049	233.862	15.293	0.015	1117.072	33.423	0.033	237.893	15.424	0.015	0.036	100.28556
	1000	$k = 5, p = 0.9$	15489.365	124.456	0.124	1145.322	33.843	0.034	2721.398	52.167	0.052	134.005	11.576	0.012	3789.021	61.555	0.062	565.714	23.785	0.024	0.051	78.7368
	1000	$k = 10, p = 0.9$	3920.077	62.611	0.063	1177.861	34.320	0.034	2349.111	48.468	0.048	189.466	13.765	0.014	1263.246	35.542	0.036	173.364	13.167	0.013	0.035	84.42318
	1000	$k = 20, p = 0.9$	4435.076	66.596	0.067	1243.404	35.262	0.035	2438.644	49.383	0.049	251.989	15.874	0.016	798.059	28.250	0.028	327.935	18.109	0.018	0.036	117.76542

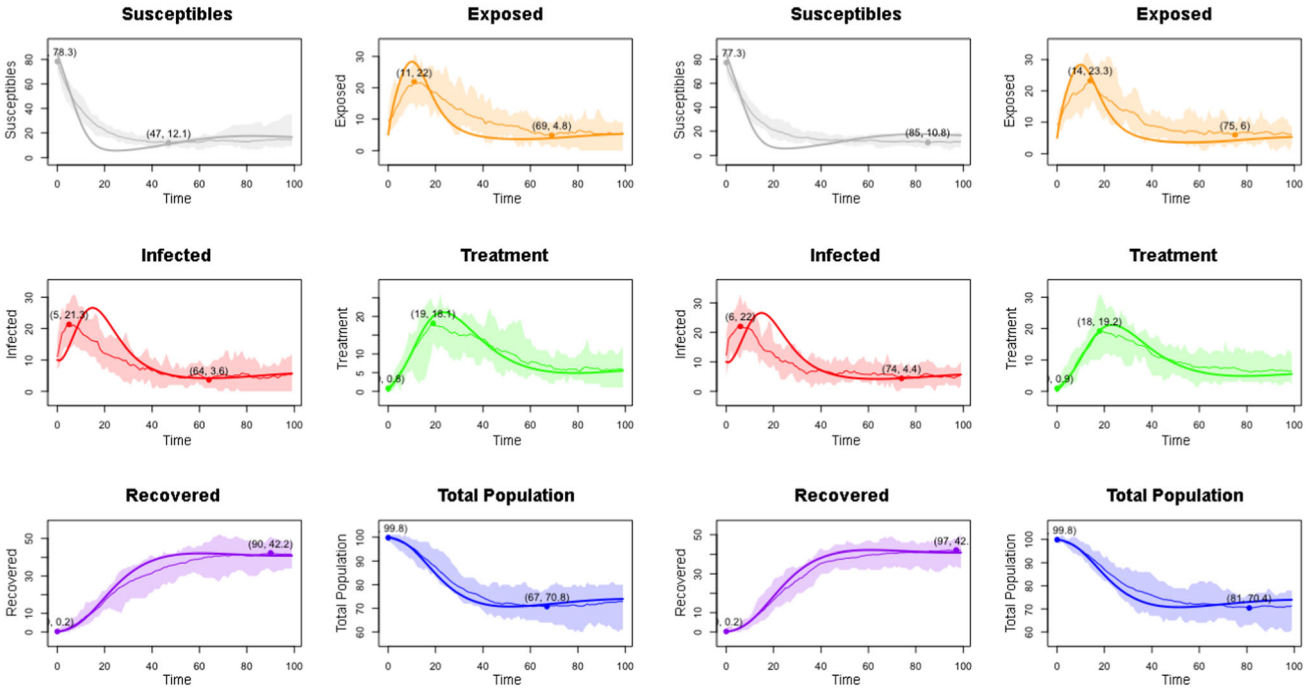

Erdős-Rényi network with n=100 and p=0.2

Erdős-Rényi network with n=100 and p=0.5

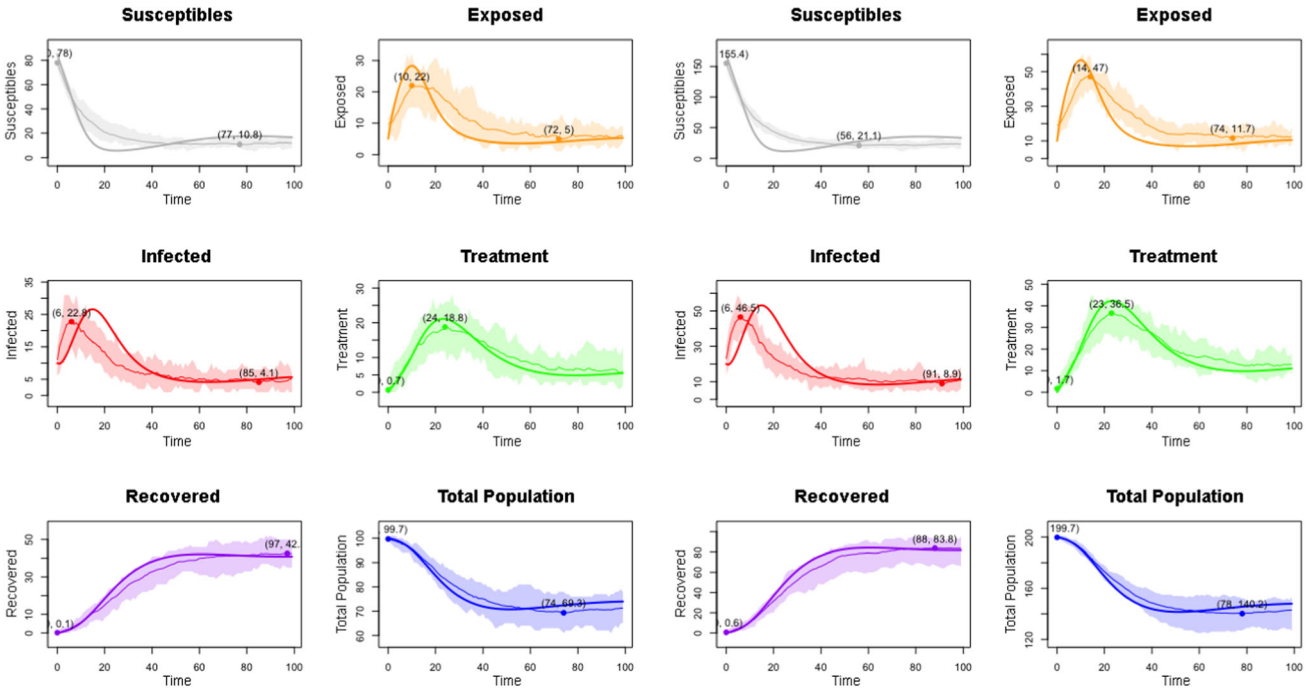

Erdős-Rényi network with n=100 and p=0.9

Erdős-Rényi network with n=200 and p=0.2

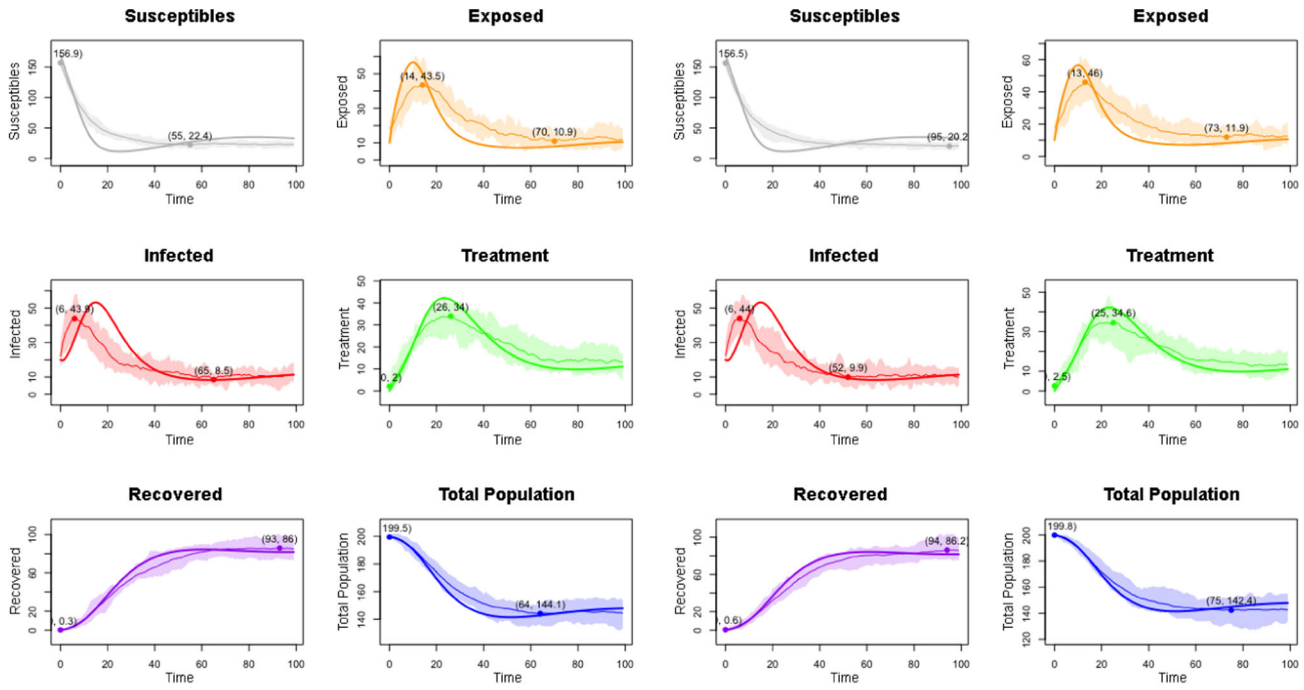

Erdős-Rényi network with n=200 and p=0.5

Erdős-Rényi network with n=200 and p=0.9

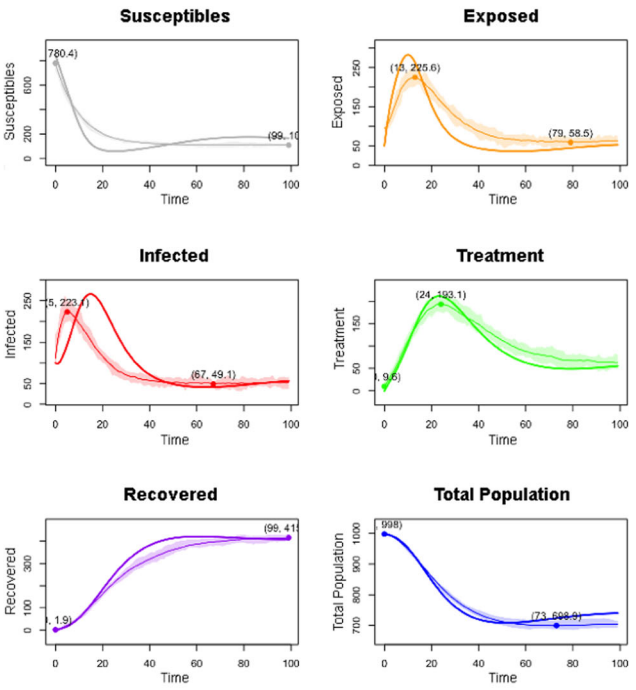

Erdős-Rényi network with n=1000 and p=0.2

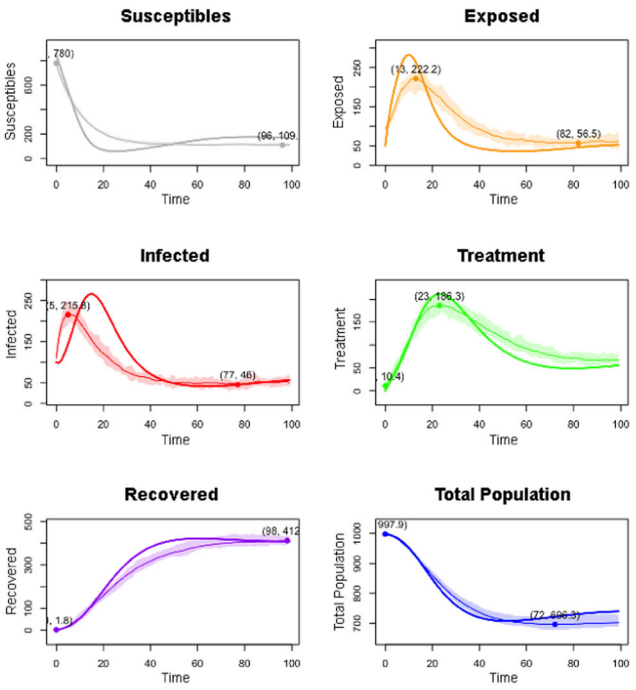

Erdős-Rényi network with n=1000 and p=0.5

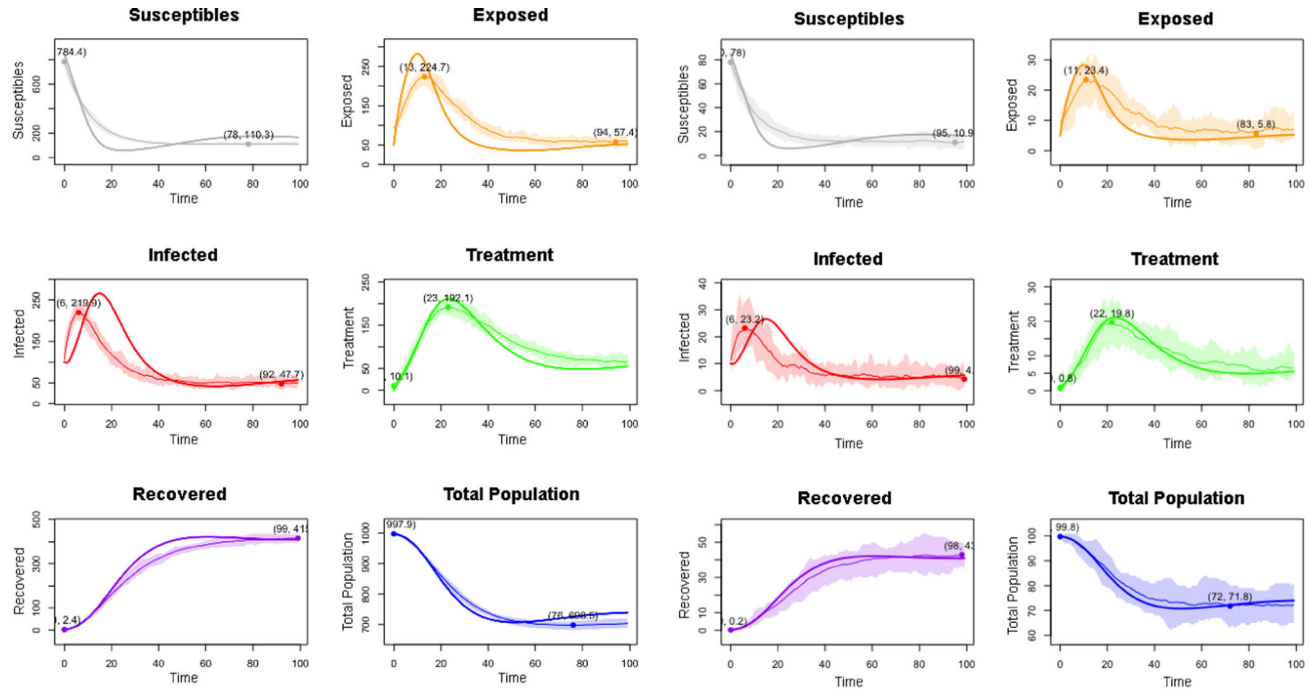

Erdős-Rényi network with n=1000 and p=0.9

Barabási–Albert network with n=100 and m=n*0.2

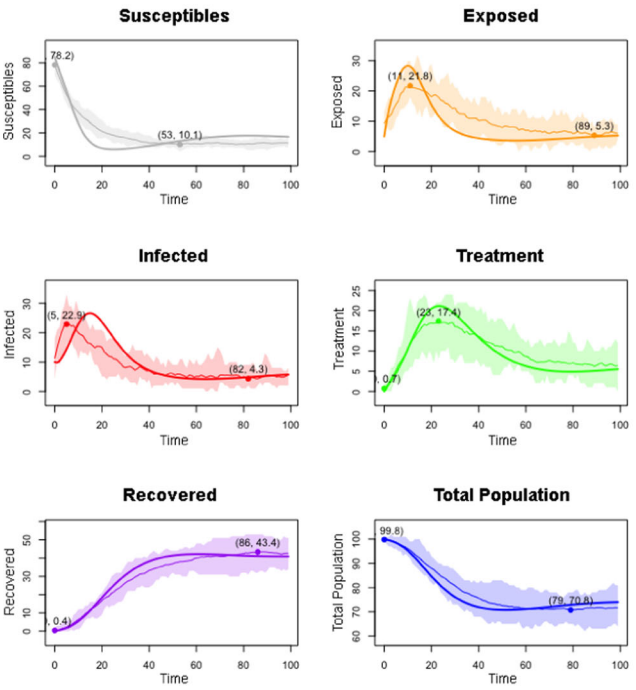

Barabási–Albert network with n=100 and m=n*0.5

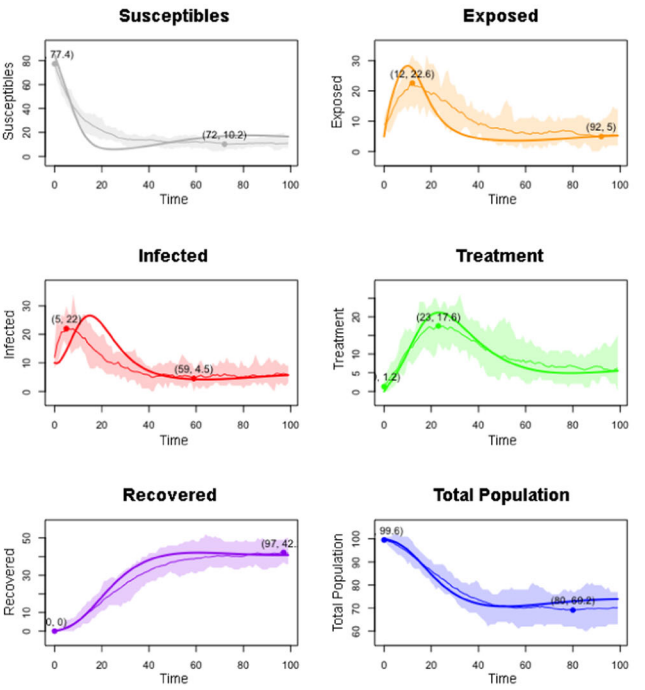

Barabási–Albert network with n=100 and m=n*0.9

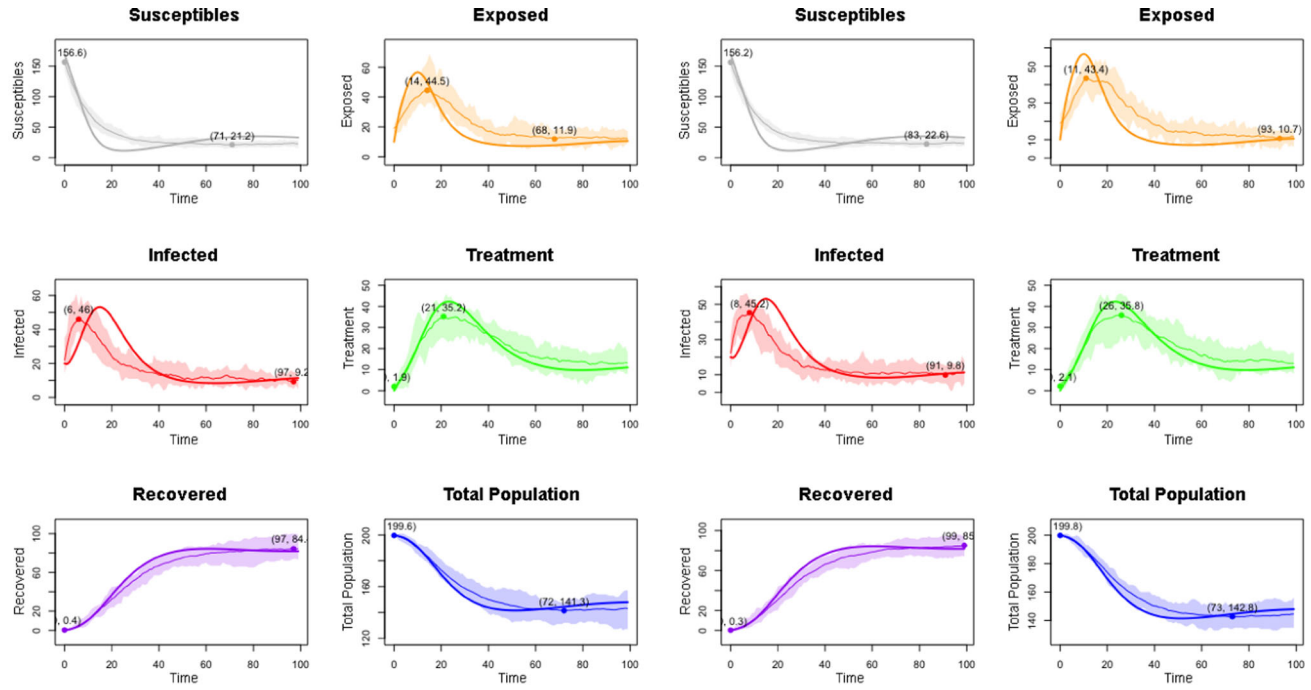

Barabási–Albert network with n=200 and m=n*0.2

Barabási–Albert network with n=200 and m=n*0.5

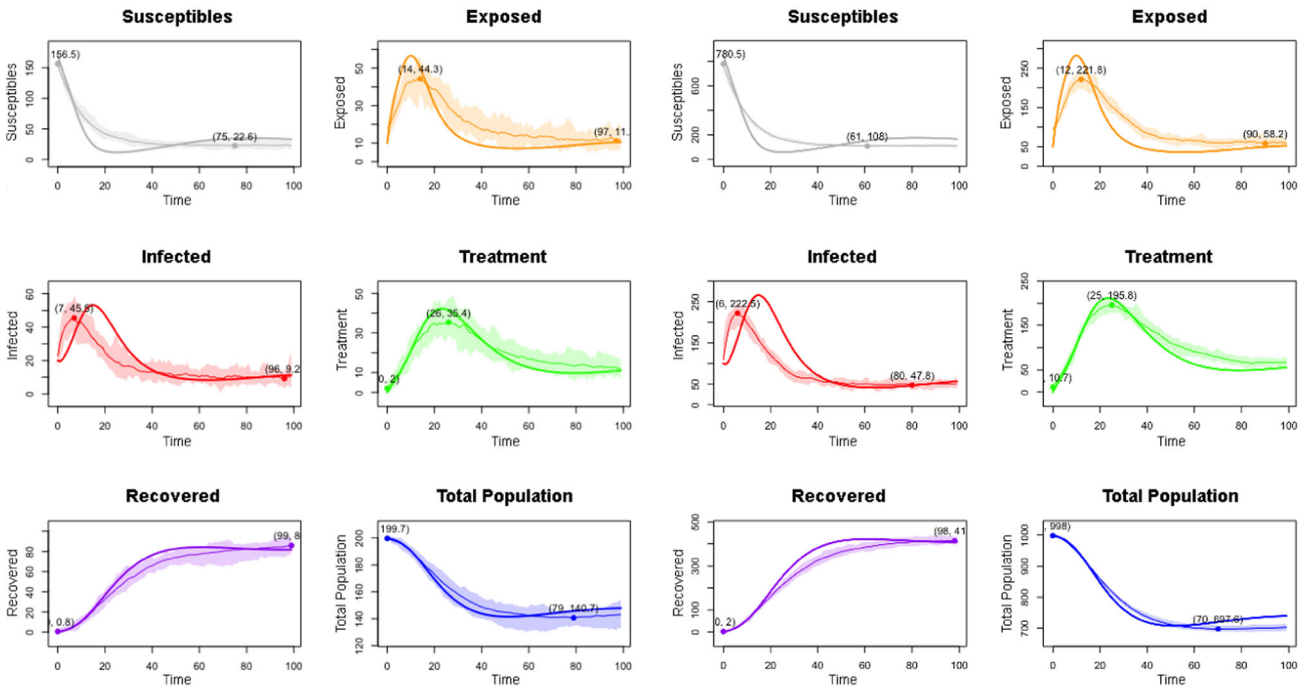

Barabási–Albert network with n=200 and m=n*0.9

Barabási–Albert network with n=1000 and m=n*0.2

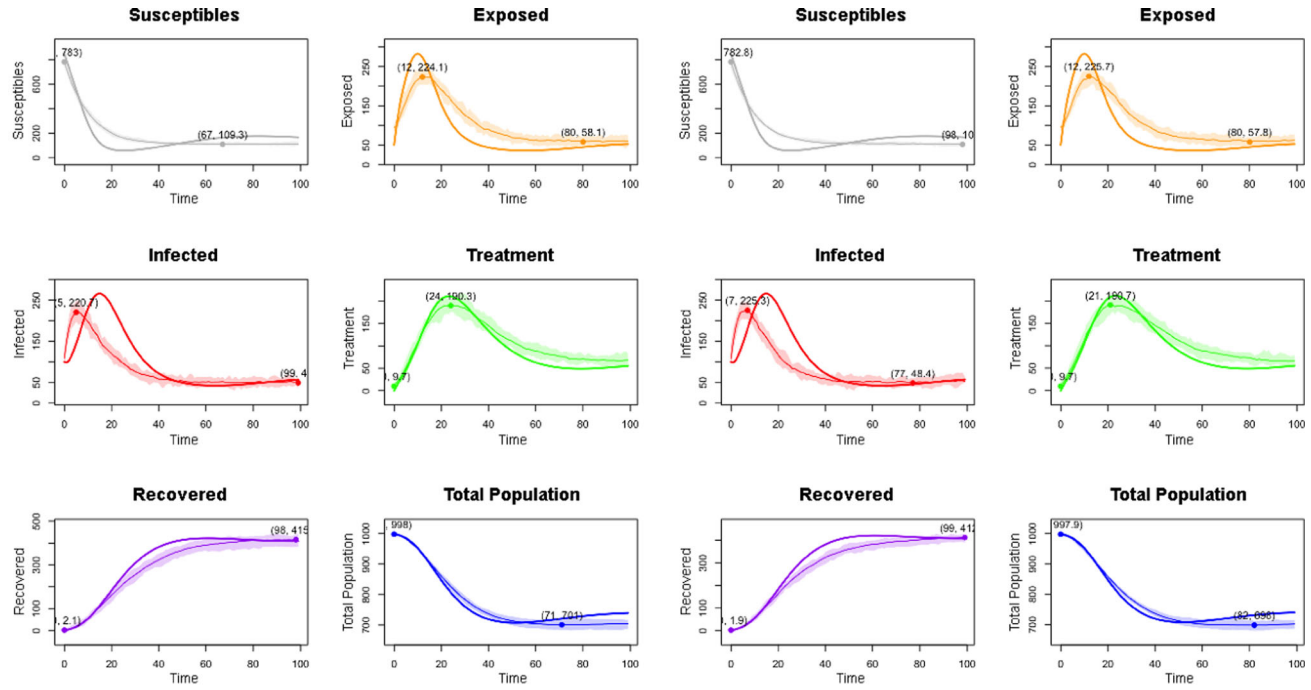

Barabási–Albert network with n=1000 and m=n*0.5

Barabási–Albert network with n=1000 and m=n*0.9

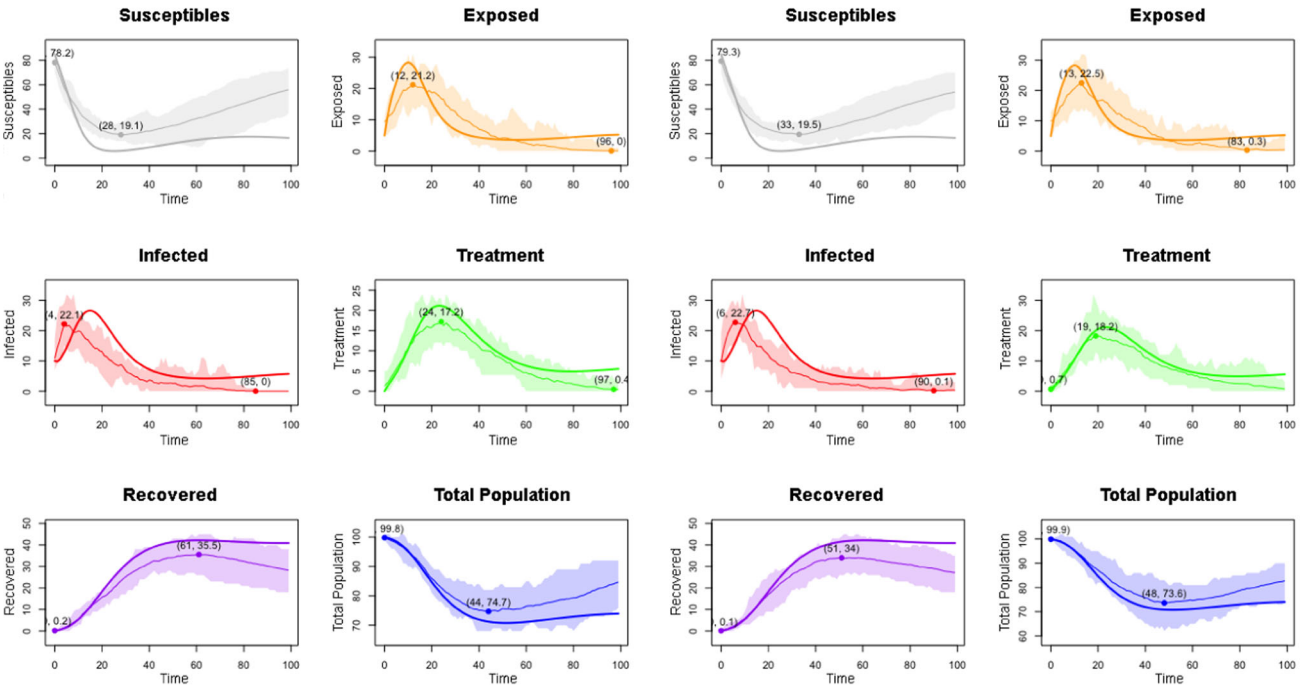

Watts-Strogatz network with n=100, k=5 and p=0.2

Watts-Strogatz network with n=100, k=5 and p=0.5

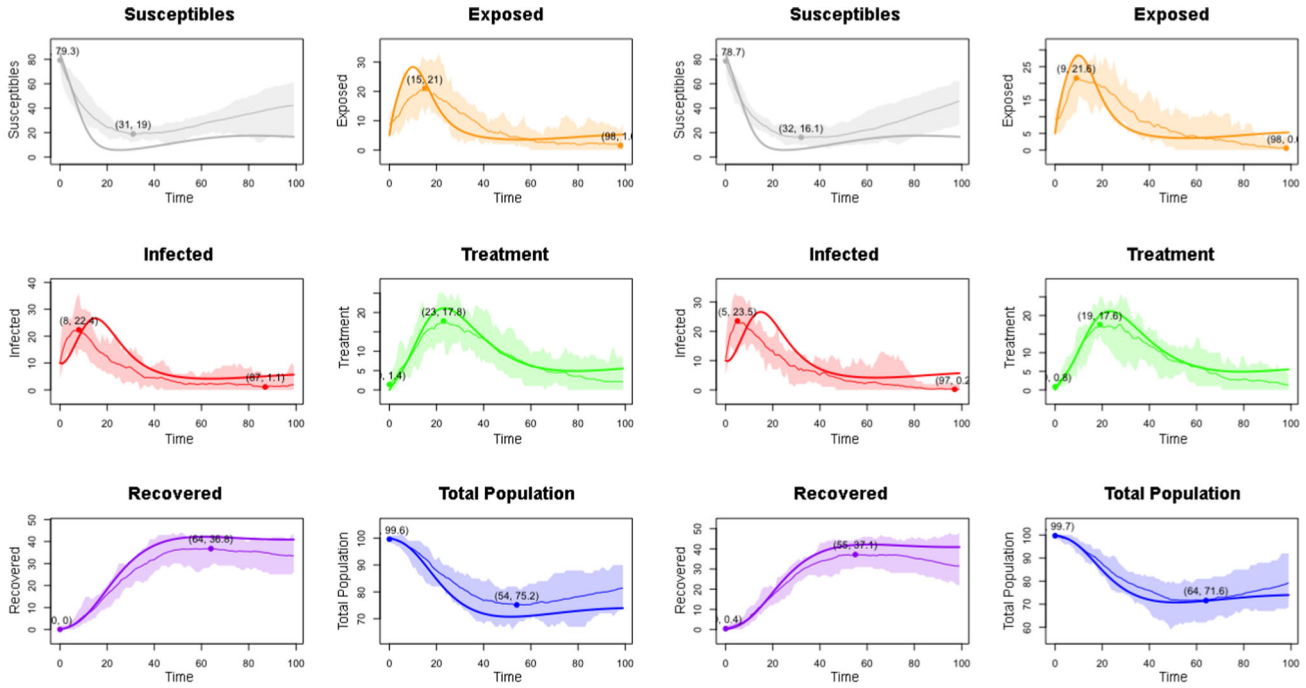

Watts-Strogatz network with n=100, k=5 and p=0.9

Watts-Strogatz network with n=100, k=10 and p=0.2

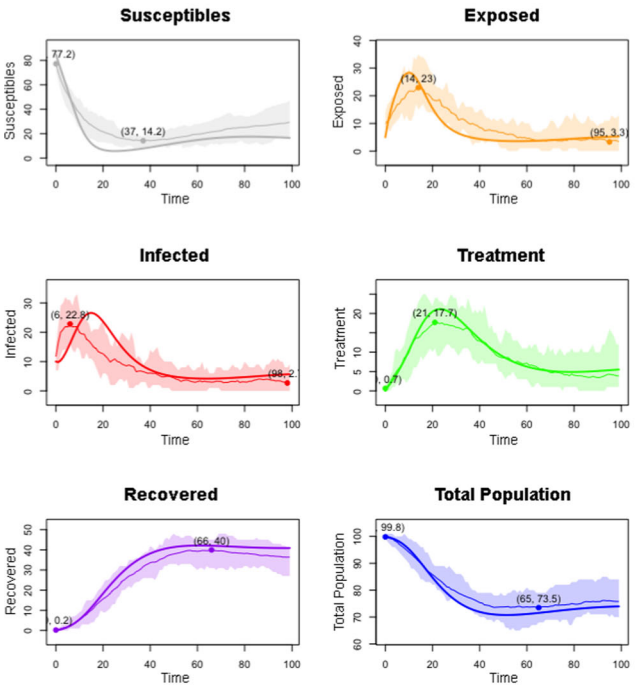

Watts-Strogatz network with n=100, k=10 and p=0.5

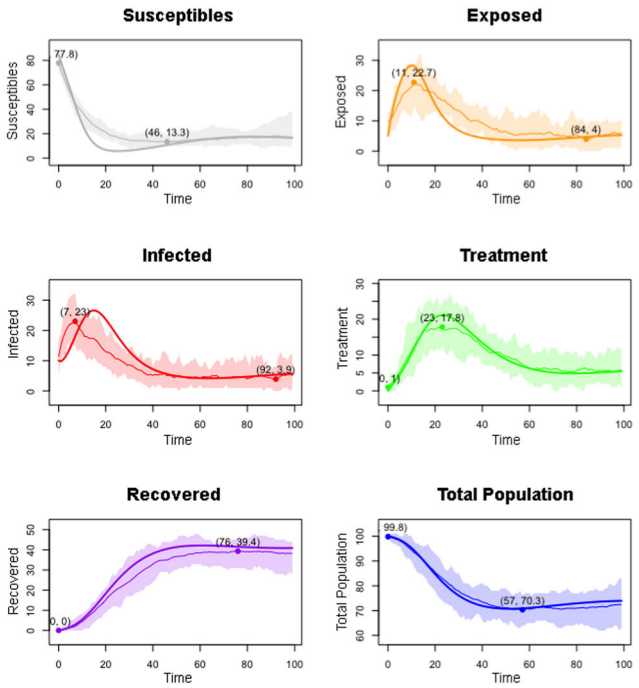

Watts-Strogatz network with n=100, k=10 and p=0.9

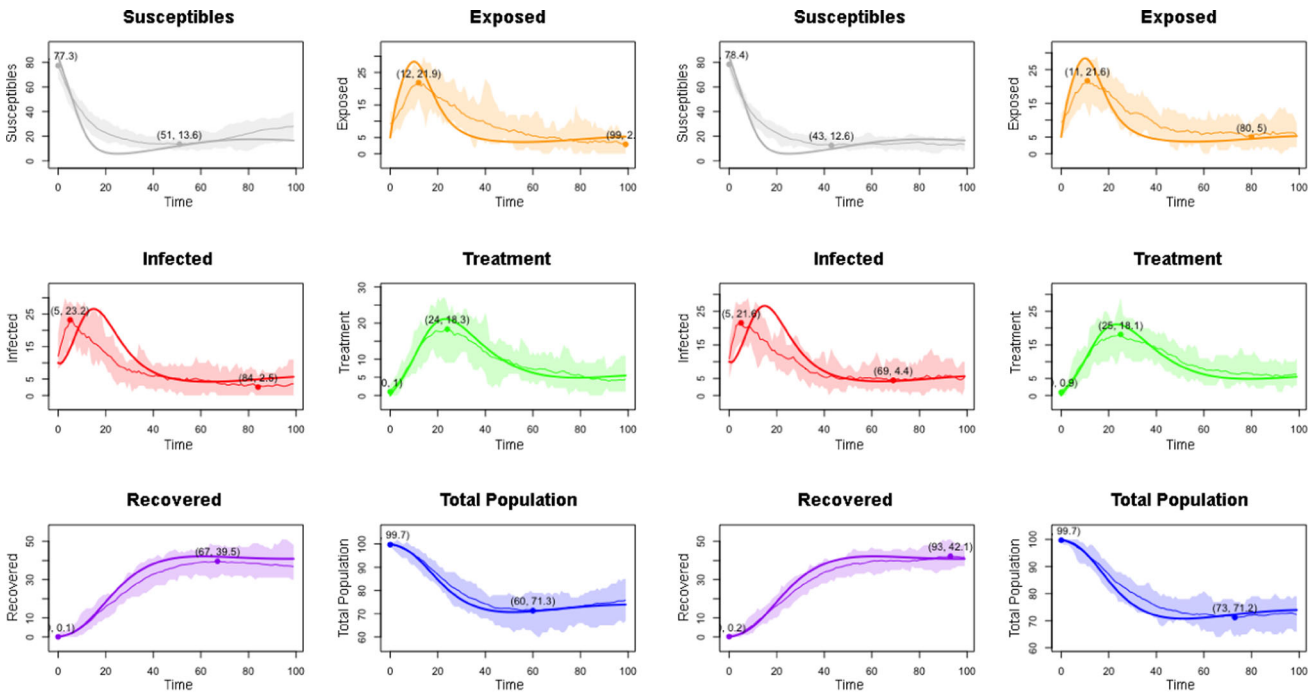

Watts-Strogatz network with n=100, k=20 and p=0.2

Watts-Strogatz network with n=100, k=20 and p=0.5

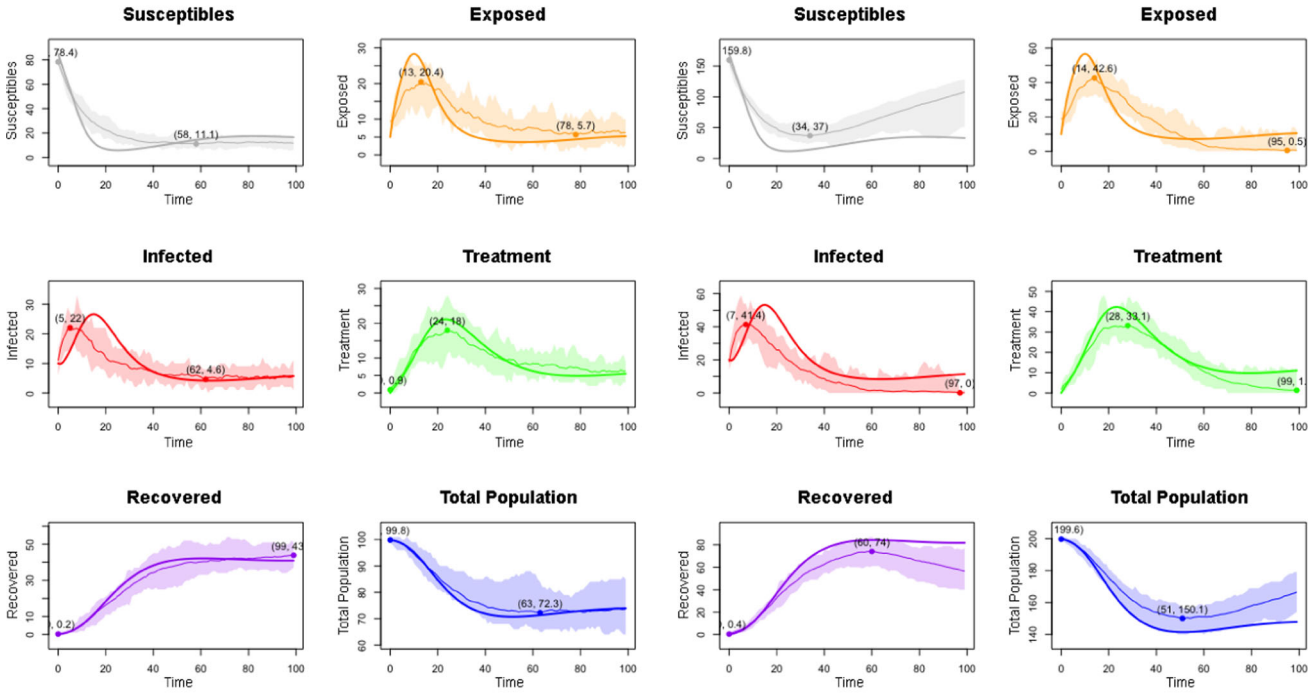

Watts-Strogatz network with n=100, k=20 and p=0.9

Watts-Strogatz network with n=200, k=5 and p=0.2

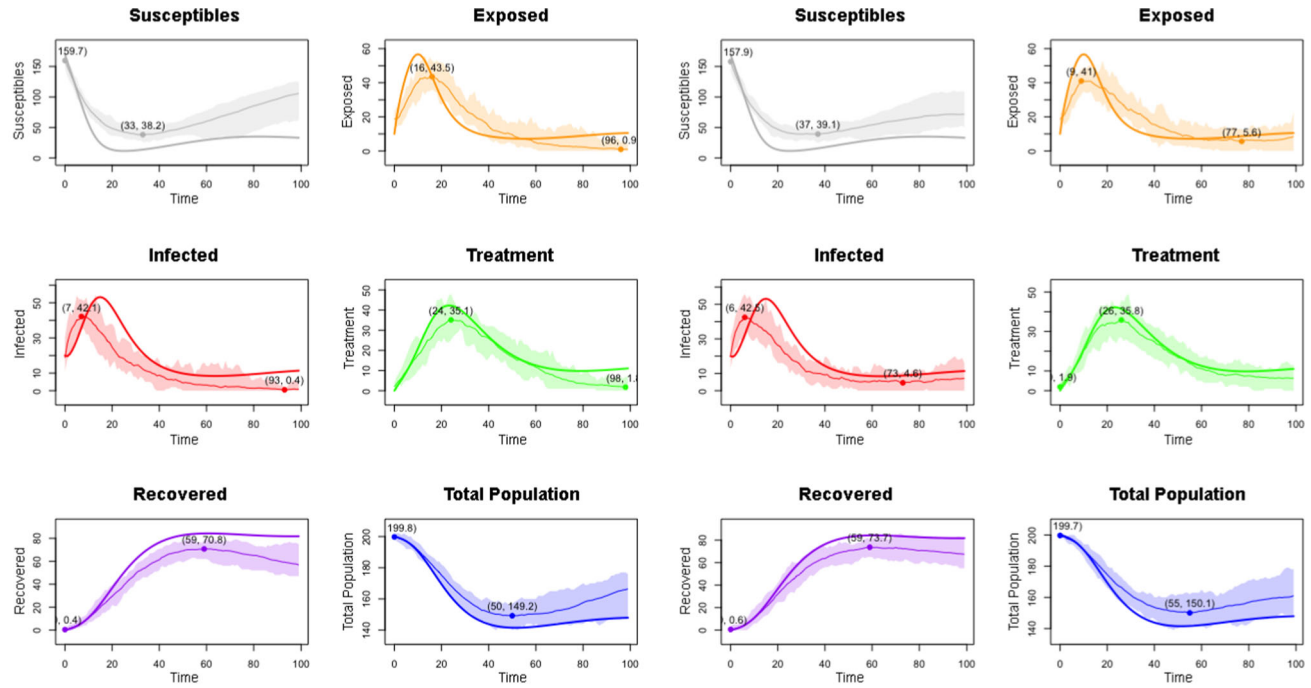

Watts-Strogatz network with n=200, k=5 and p=0.5

Watts-Strogatz network with n=200, k=5 and p=0.9

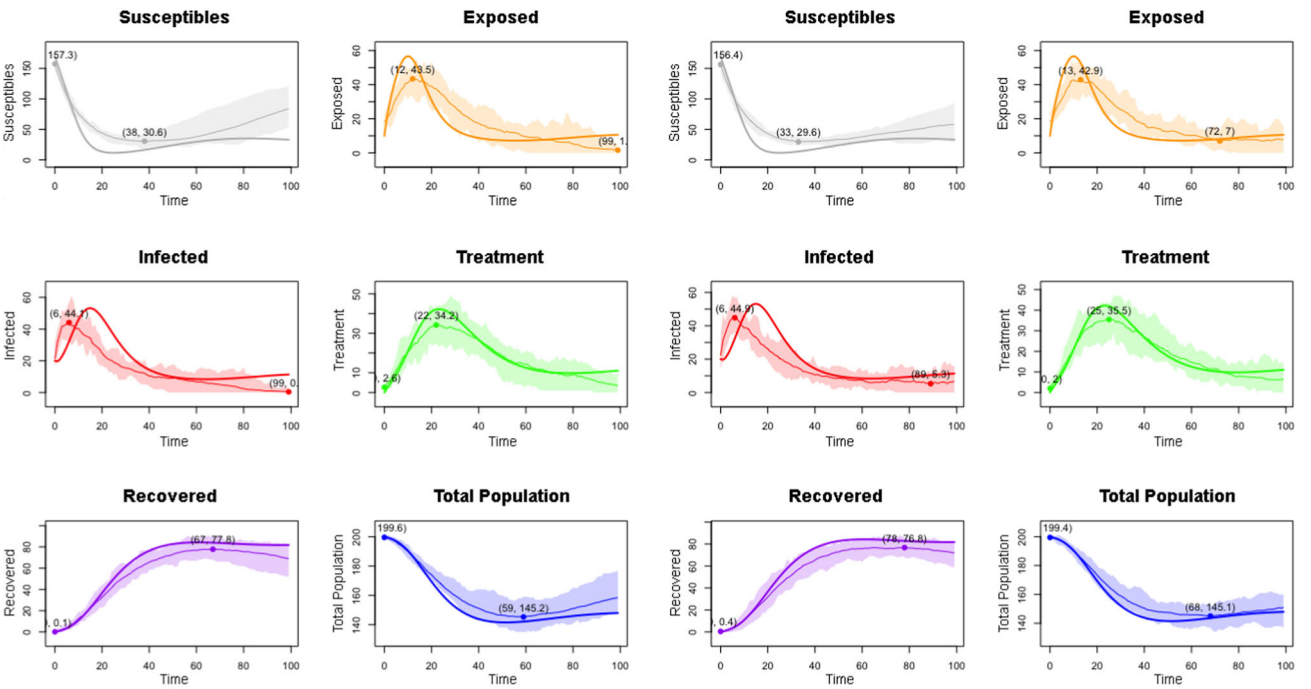

Watts-Strogatz network with n=200, k=10 and p=0.2

Watts-Strogatz network with n=200, k=10 and p=0.5

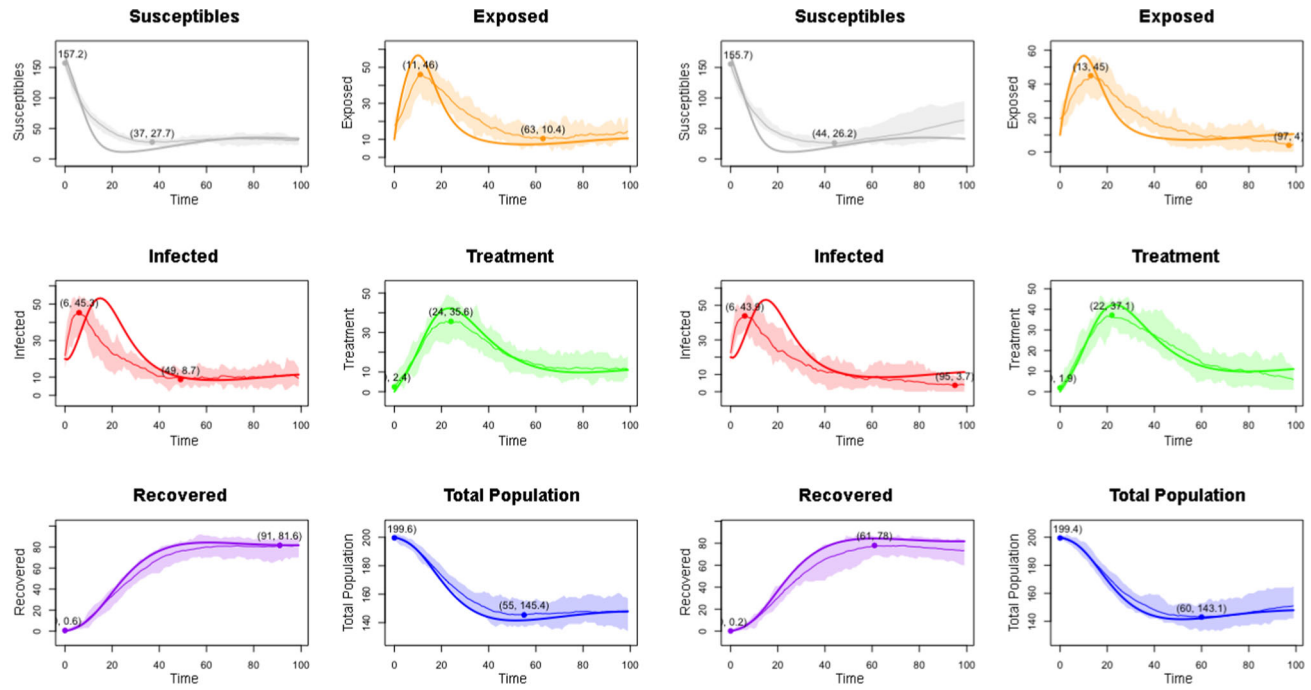

Watts-Strogatz network with n=200, k=10 and p=0.9

Watts-Strogatz network with n=200, k=20 and p=0.2

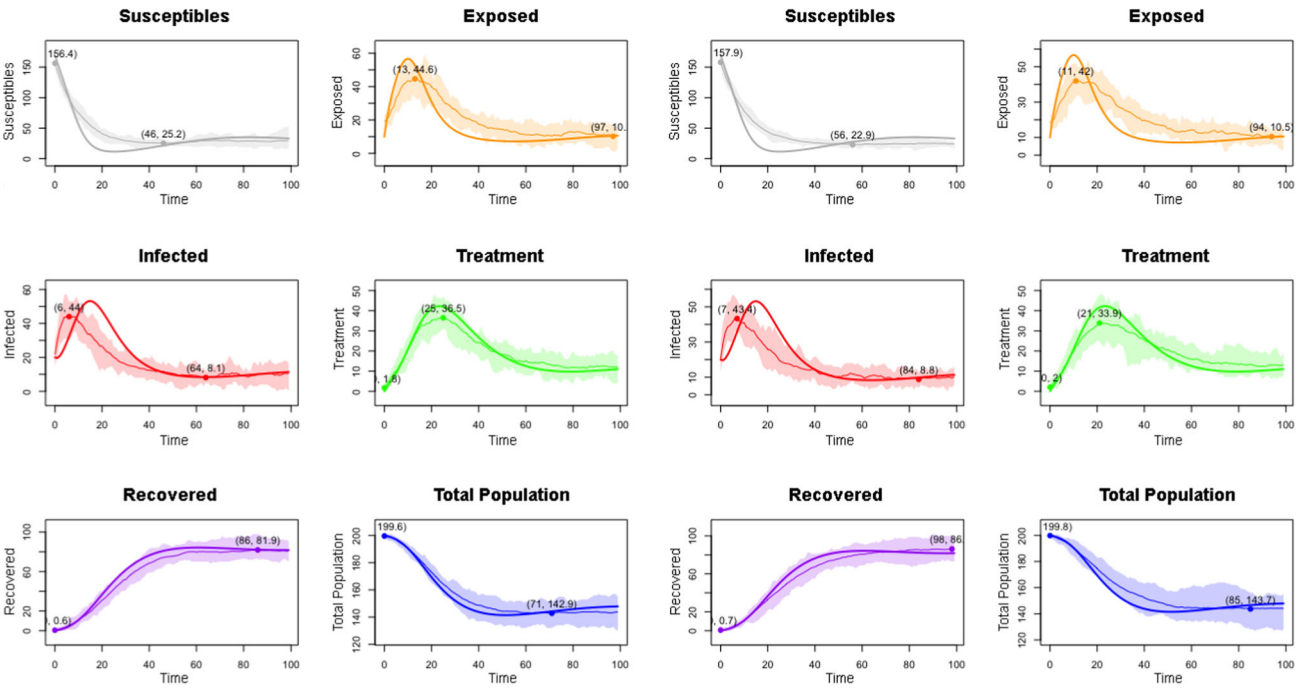

Watts-Strogatz network with n=200, k=20 and p=0.5

Watts-Strogatz network with n=200, k=20 and p=0.9

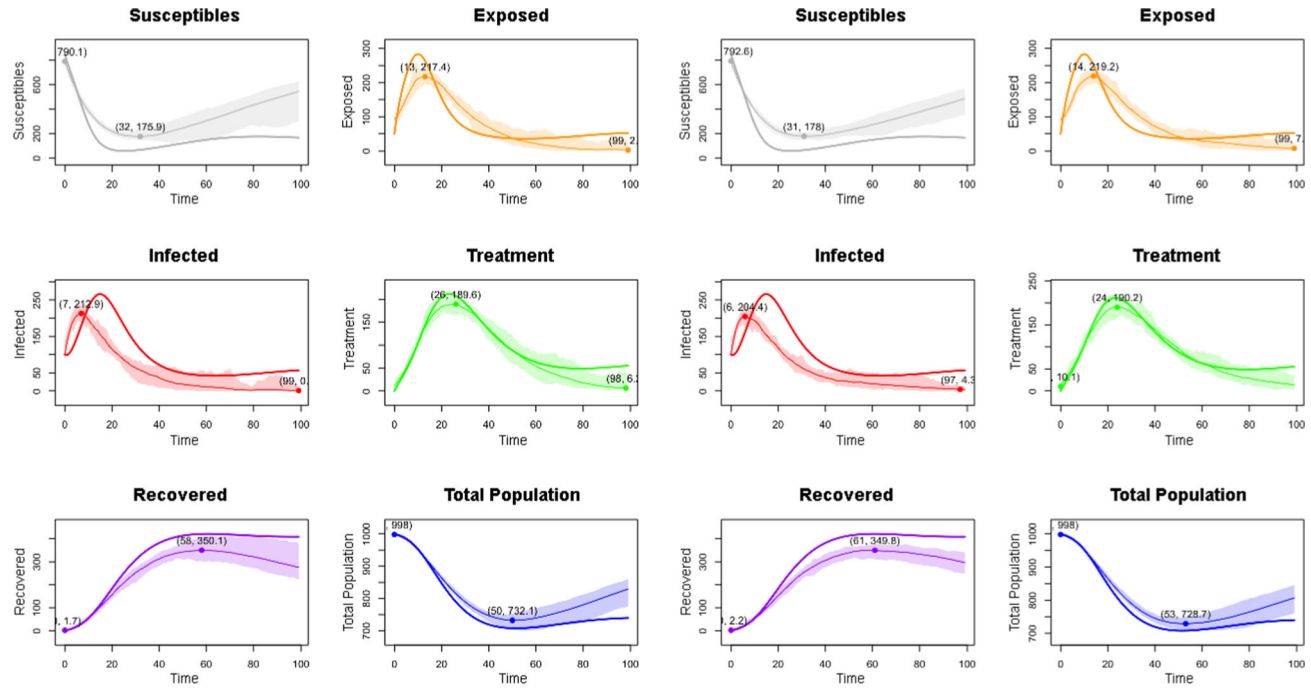

Watts-Strogatz network with n=1000, k=5 and p=0.2

Watts-Strogatz network with n=1000, k=5 and p=0.5

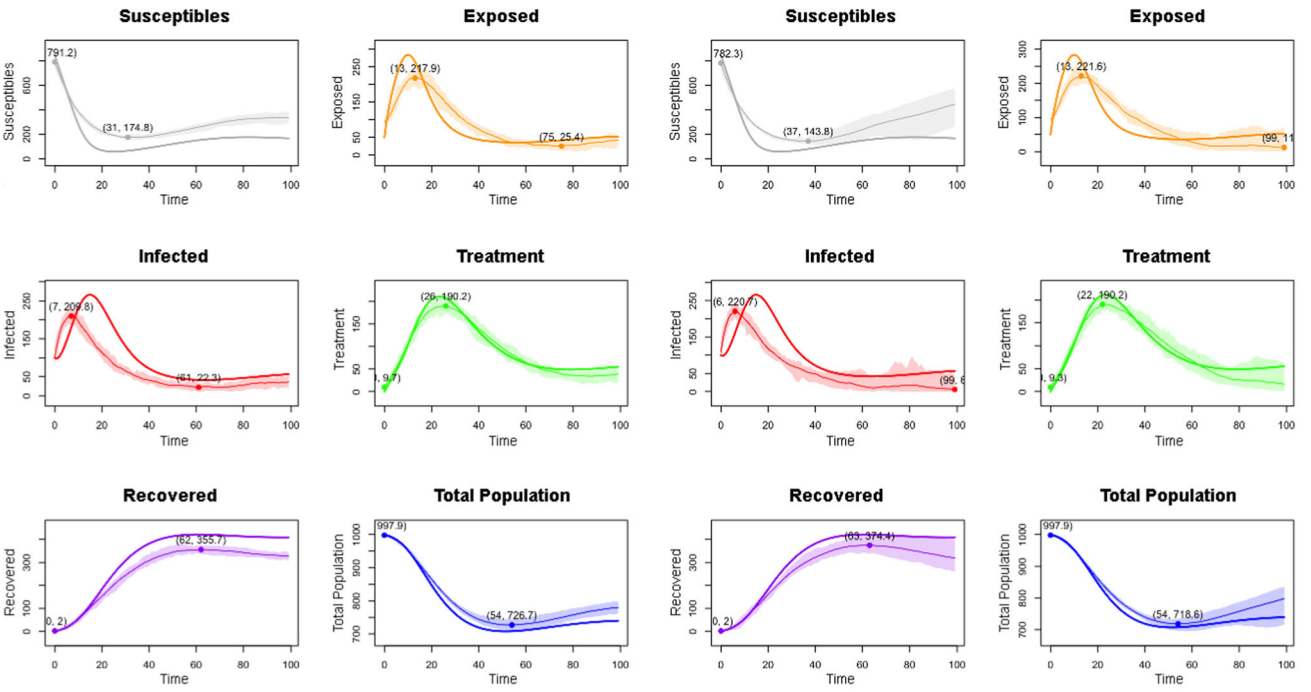

Watts-Strogatz network with n=1000, k=5 and p=0.9

Watts-Strogatz network with n=1000, k=10 and p=0.2

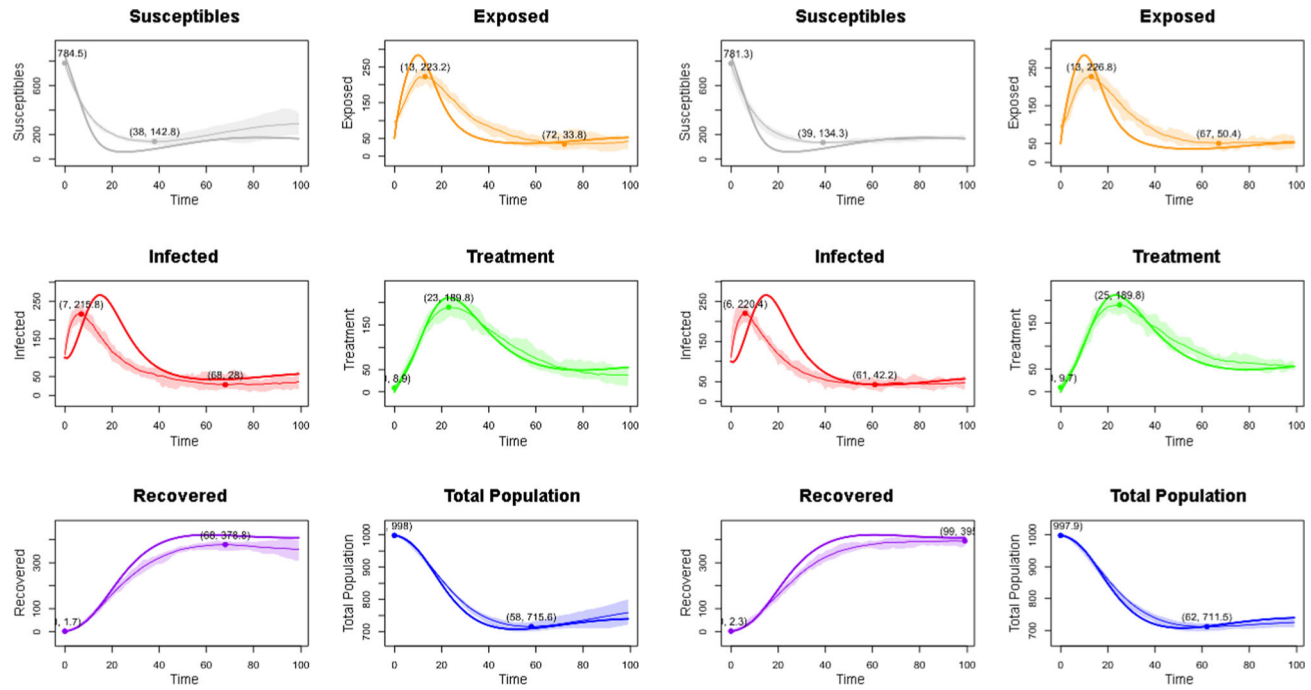

Watts-Strogatz network with n=1000, k=10 and p=0.5

Watts-Strogatz network with n=1000, k=10 and p=0.9

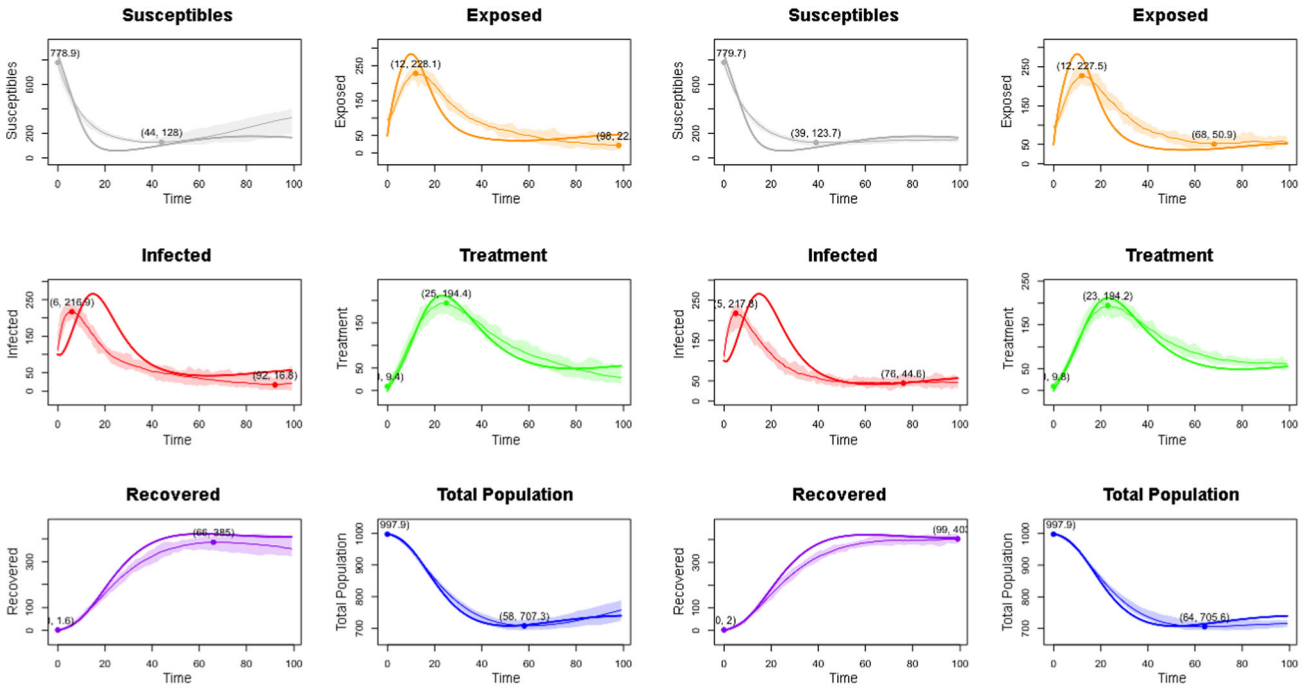

Watts-Strogatz network with n=1000, k=20 and p=0.2

Watts-Strogatz network with n=1000, k=20 and p=0.5

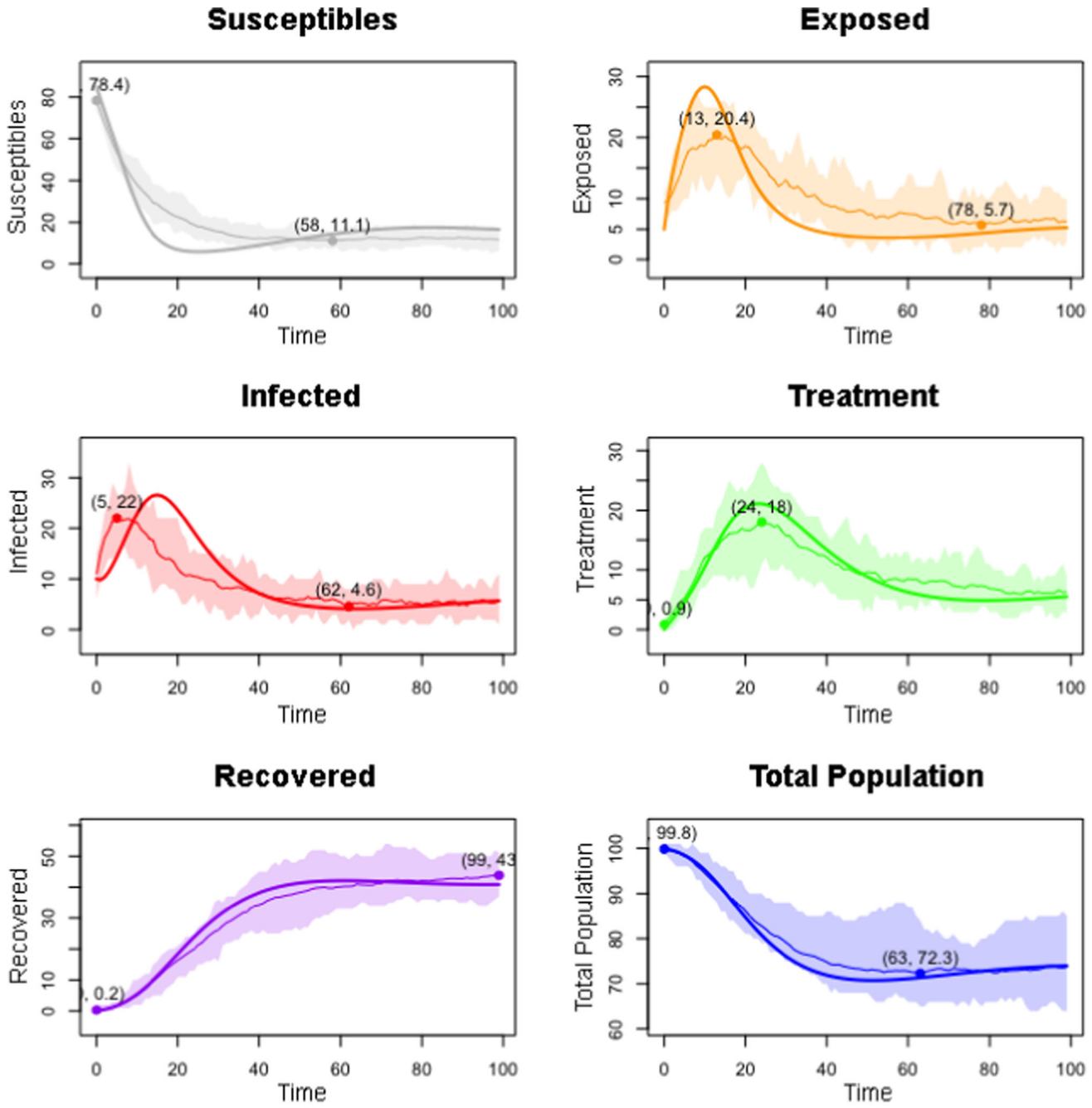

Watts-Strogatz network with n=1000, k=20 and p=0.9

References

1. K. Das, B.S.N.. Murthy, S.K. Abdus Samad, M.H. Ali Biswas, Mathematical transmission analysis of SEIR tuberculosis disease model. Sensors Int. **2**, 2666–3511 (2021)
2. M. Aguiar, V. Anam, K.B. Blyuss, C.D.S. Estadilla, B.V. Guerrero, D. Knopoff, B.W. Kooi, A.K. Srivastav, V. Steindorf, N. Stollenwerk, Mathematical models for dengue fever epidemiology: a 10-year systematic review. Phys. Life Rev. **40**, 65–92 (2022). https://doi.org/10.1016/j.plrev.2022.02.001
3. O.C. Collins, K.J. Duffy, A mathematical model for the dynamics and control of malaria in Nigeria. Infect. Dis. Model **7**(4), 728–741 (2022). https://doi.org/10.1016/j.idm.2022.10.005
4. A.I.K. Butt, M. Imran, J. Aslam, S. Batool, S. Batool, Computational analysis of control of hepatitis B virus disease through vaccination and treatment strategies. PLOS ONE **18**(10), e0288024 (2023). https://doi.org/10.1371/journal.pone.0288024
5. N. Wongvanich, I.-M. Tang, M.-A. Dubois, P. Pongsumpun, Mathematical modeling and optimal control of the hand foot mouth disease affected by regional residency in Thailand. Mathematics **9**(22), 2863 (2021). https://doi.org/10.3390/math9222863

6. A.I.K. Butt, H. Aftab, M. Imran, T. Ismaeel, Mathematical study of lumpy skin disease with optimal control analysis through vaccination. Alex. Eng. J. **2023**(72c), 247–259 (2023). https://doi.org/10.1016/j.aej.2023.03.073
7. A.I.K. Butt, H. Aftab, M. Imran et al., Dynamical study of lumpy skin disease model with optimal control analysis through pharmaceutical and non-pharmaceutical controls. Eur. Phys. J. Plus **138**, 1048 (2023). https://doi.org/10.1140/N10/s13360-023-04690-y
8. A.I.K. Butt, M. Imran, B.A. McKinney, S. Batool, H. Aftab, Mathematical and stability analysis of dengue–malaria co-infection with disease control strategies. Mathematics. (2023). https://www.mdpi.com/2554616
9. O.D. Falowo et al., Mathematical modelling of lumpy skin disease in dairy cow. IOP Conf. Ser. Earth Environ. Sci **1219**, 012007 (2023)
10. D. Khatua, D. Guha, S. Kar, A. De, E. Samanta, Analysis of SIR-network model on COVID-19 with respect to its impact on West Bengal in India medRxiv (2020). https://doi.org/10.1101/2020.08.05.20169037
11. S. Bhat, V.R. Sai, S. Mundody, R.M. Guddeti, Leveraging SIR and Barabási–Albert models for epidemic modelling. in *2024 35th conference of open innovations association (FRUCT) 2024 Apr 24*. (IEEE, 2024), pp. 170–178
12. A. Alkhazzan, J. Wang, Y. Nie, H. Khan, J. Alzabut, A stochastic SIRS modeling of transport-related infection with three types of noises. Alex. Eng. J. **1**(76), 557–72 (2023)
13. E. Kenah, J.M. Robins, Network-based analysis of stochastic SIR epidemic models with random and proportionate mixing. J. Theor. Biol. **249**(4), 706–22 (2007). https://doi.org/10.1016/j.jtbi.2007.09.011
14. M. Rafiq, A.R. Nizami, D. Baleanu, N. Ahmad, Numerical simulations on scale-free and random networks for the spread of COVID-19 in Pakistan. Alex. Eng. J. (2023). https://doi.org/10.1016/j.aej.2022.07.026
15. R. Goel, L. Bonnetain, R. Sharma, A. Furno, Mobility-based SIR model for complex networks: with case study Of COVID-19. Soc. Netw. Anal. Min. (2021). https://doi.org/10.1007/s13278-021-00814-3
16. M.J. Keeling, K.T. Eames, Networks and epidemic models. J. R. Soc. Interface **2**(4), 295–307 (2005). https://doi.org/10.1098/rsif.2005.0051
17. J. Huang, G. Qi, Effects of control measures on the dynamics of COVID-19 and double-peak behavior in Spain. Nonlinear Dyn. **101**(3), 1889–1899 (2020). https://doi.org/10.1007/s11071-020-05901-2
18. M. Emmerich, Y. Kuryliak, D. Dosyn. Simulation of the effects of targeted immunization on the peak number of infections in complex networks. (InMoMLeT+ DS, 2022), pp. 1–13
19. Y. Kuryliak, M. Emmerich, D. Dosyn, Efficient stochastic simulation of network topology effects on the peak number of infections in epidemic outbreaks (2022). arXiv preprint arXiv:2202.13325
20. P. Erdős, A. Rényi, On random graphs I. Publ. Math. Debr. **6**(290–297), 18 (1959)
21. A.L. Barabási, R. Albert, Emergence of scaling in random networks. Science **286**(5439), 509–512 (1999)
22. J.D. Watts, S.H. Strogatz, Collective dynamics of 'small-world' networks. Nature **393**(6684), 440–442 (1998)